Atmos. Chem. Phys. Discuss., 12, 28385–28450, 2012
www.atmos-chem-phys-discuss.net/12/28385/2012/
doi:10.5194/acpd-12-28385-2012

Atmospheric Chemistry and Physics Discussions

Assessment of atmospheric processes driving ozone variations in the subtropical North Atlantic free troposphere

E. Cuevas[1], Y. González[1], S. Rodríguez[1], J. C. Guerra[2], A. J. Gómez-Peláez[1], S. Alonso-Pérez[1,3], J. Bustos[1], and C. Milford[4,1]

[1]Izaña Atmospheric Research Centre (IARC), Agencia Estatal de Meteorología (AEMET), Izaña, Spain
[2]La Laguna University, Hydrometeorology Research Group (GRIHM), (ULL), Cuesta, Spain
[3]Institute of Environmental Assessment and Water Research (CSIC), Barcelona, Spain
[4]University of Huelva, Joint Research Unit to CSIC (UHU), Huelva, Spain

Received: 1 July 2012 – Accepted: 11 October 2012 – Published: 30 October 2012

Correspondence to: E. Cuevas (ecuevasa@aemet.es)

Published by Copernicus Publications on behalf of the European Geosciences Union.

Abstract

An analysis of the 22-yr ozone (O_3) series (1988–2009) at the subtropical high mountain Izaña station (IZO; 2373 m a.s.l.), representative of free troposphere (FT) conditions, is presented. Diurnal and seasonal O_3 variations as well as the O_3 trend ($0.19 \pm 0.05\,\%\,yr^{-1}$ or $0.09\,ppbv\,yr^{-1}$), are assessed. A climatology of O_3 transport pathways using backward trajectories shows that higher O_3 values are associated with air masses traveling above 4 km altitude from North America and North Atlantic Ocean, while low O_3 is transported from the Saharan continental boundary layer (CBL). O_3 data have been compared with PM_{10}, ^{210}Pb, ^{7}Be, potential vorticity (PV) and carbon monoxide (CO). A clear negative logarithmic relationship was observed between PM_{10} and surface O_3 for all seasons. A similar relationship was found between O_3 and ^{210}Pb, but only for the summer-time. The highest daily O_3 values (90th percentile) are observed in spring and in the first half of summer-time. A positive correlation between O_3 and PV, and between O_3 and ^{7}Be is found throughout the year, indicating that relatively high surface O_3 values at IZO originate from the middle and upper troposphere. At IZO we find a good correlation between O_3 and CO in winter, supporting the hypothesis of long-range transport of photochemically generated O_3 from North America. Aged air masses, in combination with sporadic inputs from the upper troposphere, are observed in spring, summer and autumn. In summer-time high O_3 values seem to be the result of stratosphere-to-troposphere (STT) exchange processes in regions neighbouring the Canary Islands. Since 1995–1996, the North Atlantic Oscillation has changed from a predominantly high positive phase to alternating between negative, neutral or positive phases. This change results in an increased flow of the westerlies in the mid-latitude and subtropical North Atlantic, thus favouring the transport of O_3 and its precursors from North America, and a higher frequency of storms over North Atlantic, with a likely higher incidence of STT processes in mid latitudes. These processes lead to an increase of tropospheric O_3 in the subtropical North Atlantic region after 1996 that has been reflected in surface O_3 records at IZO.

ACPD
12, 28385–28450, 2012

1 Introduction

Ozone (O_3) is an important trace gas in the troposphere (Fishman and Crutzen, 1978). It affects the oxidizing capacity of the troposphere (Levy, 1971; Logan, 1985; Thompson, 1992), it is a phytotoxicant that can affect public health (Tiao et al., 1975), and is an important greenhouse gas (Ramanathan et al., 1985; Mitchel, 1989). A portion of the O_3 is downward transported from the stratosphere (Junge, 1962; Danielsen, 1968; Levy et al., 1985), while most of the tropospheric O_3 is believed to be produced in the troposphere itself by photochemical reactions involving nitrogen oxides (NO_x) and carbon monoxide (CO) (Lelieveld and Dentener, 2000; Jonson et al., 2006). Thus, O_3 concentrations may be viewed as the sum of a global/hemispheric background concentration and regionally/locally produced O_3 (Jonson et al., 2006).

Results from Graustein and Turekian (1996) indicate an upper troposphere source for elevated O_3 in summer-time subtropical free troposphere (FT) of the Eastern North Atlantic, and James et al. (2003) found evidence of deep stratospheric intrusions down to the lower FT over the Canaries even in summer. Oltmans et al. (1996) reported evidence of high O_3 concentration ($\sim$ 100 ppb) layers in the middle and upper troposphere over the North Atlantic which are invariably associated with transport characteristics that strongly support a stratospheric source for these layers.

However, other authors (e.g. Moody et al., 1996; Creilson et al., 2003; Hegarty et al., 2009) suggest that a substantial amount of photochemically generated tropospheric O_3 is transported from continental source regions over the North Atlantic. Some studies have revealed the great impact of this pollution over the air quality of Europe (e.g. Li et al., 2002a; Prather et al., 2003; Parrish et al., 1993). As pointed out by Stohl (2001) and Stohl et al. (2002) the long-range transport of O_3 from North America to Europe is more efficient in the middle and upper FT because the westerlies are stronger than in the marine boundary layer (MBL), and because of a longer O_3 lifetime. Val Martin et al. (2008) suggest that a substantial amount of additional O_3 formation occurs in the anthropogenic plumes during transport to the Central North Atlantic lower FT.

ACPD
12, 28385–28450, 2012

Assessment of long-term trends in tropospheric O_3 is difficult due to the scarcity of representative observing sites with long records (Solomon et al., 2007). In addition, the long-term tropospheric O_3 trends vary both in terms of sign and magnitude and in the possible causes of the change (Oltmans et al., 2006). Some O_3 trends have been attributed to changes in O_3 precursor emissions (Scheel, 1983). However further studies reveal that O_3 trends cannot be fully explained based on its precursors alone. For example, Staehelin and Poberaj (2008) argue that further increase in background O_3 over Europe and North America since the early 1990s cannot be solely explained by regional O_3 precursor changes because anthropogenic O_3 precursor emissions were drastically reduced in the industrialized countries as a consequence of air quality legislation. Gilge et al. (2010) also state the apparent contradiction between the rather constant O_3 concentrations observed at ground stations during the end of the 1990s to 2007 and the substantial reductions in anthropogenic emissions. The surface O_3 positive trend found at elevated European sites was explained by Ordóñez et al. (2007) in terms of an increased contribution of stratospheric O_3 in the 90s. Conversely, Tarasova et al. (2003) found negative trends in a high mountain in Russia, and Vingarzan (2004) and Tarasova et al. (2009) reported a slower rate of tropospheric O_3 increase or in some cases lack of an increase over the past decade. Spatial and temporal evolution of atmospheric processes driving O_3 concentrations affect stations located in different regions of the world in different ways. In this regard, Jonson et al. (2006) address the question if the observed O_3 trends can be understood.

Model simulations suggest that the increase of background tropospheric O_3 observed in mountain tops can be only partially explained by changes in emissions of precursors over continents, and may be affected by changes in the circulation of the troposphere (Jonson et al., 2006). For example, Appenzeller et al. (2000) found a good correlation between the North Atlantic Oscillation (NAO) index and column tropospheric O_3 over Eastern North Atlantic, and Eckhardt et al. (2003) demonstrated how the NAO controls the air pollution transport to the Arctic. Duncan and Bey (2004) explained that the CO burden from Europe tended to be higher over the North Atlantic and lower over

ACPD
12, 28385–28450, 2012

the Arctic when the NAO was in the negative phase. So, reductions in O_3 caused by reductions in precursors may be masked by periodical changes in atmospheric circulation. As noted by Jonson et al. (2006), the changes suffered by the stratospheric O_3 in the last decades could alter the circulation patterns, which would affect, in turn, the exchange between the stratosphere and troposphere.

Most of the studies address the origin of tropospheric ozone from only one of the most common approaches: photochemistry or atmospheric dynamics, which is a limited and partial view of the driving forces. So, we propose, firstly, a detailed analysis of a long-term (22 yr) surface O_3 time series (1988–2009) at the Izaña high mountain station (hereafter IZO), which is representative of background conditions of the lower troposphere in the subtropical North Atlantic region, where there is very little information available. Secondly, we present an extensive and multidisciplinary review of the O_3 transport processes into the FT of the North Atlantic subtropical region, incorporating other components such as particulate matter, CO, ^{7}Be, ^{210}Pb, and additional information from backward trajectories, potential vorticity (PV), and NAO index.

The surface O_3 measurement programme of IZO is run with an independent quality assurance system, within the World Meteorological Organization (WMO) Global Atmospheric Watch (GAW) Programme, which precludes data biases and prevents wrong interpretations in trends analysis. Our paper is structured as follows: data and methods are described in Sect. 2. In Sect. 3 a surface O_3 climatology and transport pathways characterization is presented, and a discussion about surface O_3 observations, their relationships with other atmospheric components (PM_{10}, ^{210}Pb, PV, ^{7}Be, and CO), and their connections with synoptic scale dynamical processes driven by the NAO is given. In Sect. 4 a summary and main conclusions are provided.

ACPD
12, 28385–28450, 2012

2 Data and methods

2.1 Measurement site

The Izaña GAW Observatory is located at 28.3° N, 16.5° W at an altitude of 2373 m a.s.l. (annual mean pressure of ~770 hPa) on Tenerife Island, (Canary Islands, Spain) on top of a mountain platform on a dorsal ridge which crosses the island from SW to NE. A belt of endemic pine forest (*Pinus Canariensis* CHr, Sm. Ex DC) grows between 600 and 2000 m a.s.l., whereas at higher levels there is only a sparse cover of local species of broom (*Spartocytisus supranubius*) growing on lava terrain. Except for a few scattered residences, Tenerife is uninhabited above the 1000 m level. The horizontal distances from IZO to the northwest and to the southeast coasts (the direction of the prevailing winds) are less than 15 km. The nearest distance to the European continent is 1300 km and about 350 km to Africa.

2.2 In situ surface O_3 instrumentation

The surface O_3 monitoring programme at IZO started in May 1987 using UV-absorption technique. The analyzers used in different periods from then to now, as well as the reference instruments and the quality assurance programmes are specified in Table 1. The terminology used in Table 1 is the following:

- Basic instrument: analyzer from which the final data result.
- Backup instrument: instrument that is monitoring in parallel to the basic analyzer.
- Reference instrument: analyser for independent comparisons and calibrations (not used for ambient air measurements).

O_3 has been measured continuously recording 10-min averages with the corresponding standard deviation from May 1987 to July 1996. After this date, and up to now, 1-min average O_3 values with corresponding standard deviations are recorded for both

ACPD
12, 28385–28450, 2012

the basic and the backup instruments. Zero-checks with an activated-carbon absorber were performed on a daily basis to detect instrumental offset drifts. Surface O_3 data at IZO have been also calibrated against references that are traceable to NIST (US National Institute for Standards and Technology) reference O_3 photometer (Gaithersburg-Maryland, USA). The Izaña surface O_3 programme has been audited by the World Calibration Centre for Surface Ozone, Carbon Monoxide and Methane (WCC-Ozone-CO-CH4-EMPA) in 1996, 1998, 2000, 2004 and 2009. EMPA's audit reports are available at http://www.empa.ch/gaw/audits/IZO_yyyy.pdf, where yyyy is the year. The audits were performed according to the "Standard Operating Procedure (SOP) for performance auditing O_3 analysers at global and regional WMO-GAW sites", WMO-GAW Report No. 97. All audited field instruments (basic and backup instruments) fulfilled the assessment criteria as "good" over the tested range up to 100 ppbv.

2.3 Backward trajectories, O_3 MCAR plots, residence times, and BTMH plots

Five-day HYSPLIT (Hybrid Single-Particle Lagrangian Integrated Trajectory) version 4.0 dispersion model backward trajectories (Draxler and Rolph, 2003; Rolph, 1983), with a time resolution of 1h were calculated using the FNL (Final Analysis Data) meteorological data-set (from May 1987 to December 2004) and the GDAS (Global Data Assimilation System) meteorological data-set (from January 2004 to December 2009), both from the National Centres for Environmental Prediction. The vertical component of the backward trajectories was computed using the vertical model velocity. The end-point was set at Tenerife (28.3° N, 16.5° W) at 2400 m a.s.l. (IZO height) for each day of the study period (1 January 1988–31 December 2009) at 00:00 UTC.

The transport paths of the air masses reaching Tenerife (00:00 UTC) have been characterized using the permanence indexes for the predefined source geographic sectors described in Alonso-Pérez et al. (2007) and summarized in Table 2. Permanence indexes were calculated as the fraction of time that an air mass trajectory calculated for 120 h resides in a pre-defined particular geographic sector and also in a predefined altitude range. We consider "low" an altitude range between surface level and 1.5 km,

ACPD
12, 28385–28450, 2012

"medium" an altitude range between 1.5 and 3 km, and "high" > 3 km (normally with a top-height at 6 km). Permanence indexes were obtained using 5-day HYSPLIT backward trajectories.

Mean Concentrations At Receptor (MCAR) plots allowed the identification of pathway regions with high and low O_3. MCAR plots represent the mean O_3 concentration, recorded at IZO, when air masses passed above each $1^\circ \times 1^\circ$ cell. The methodology has been described by Rodríguez et al. (2011). Monthly MCAR plots of surface O_3 were determined using daily 5-day backward trajectories calculated at 00:00 UTC and daily (nocturnal) surface O_3 data at IZO for the period 1988–2009.

The identification of the transport corridors and source regions of O_3 was complemented by using the residence time analysis technique (Poirot and Wishinski, 1986). For this issue, the geophysical region covered by the trajectories was divided into 408 grid cells of $5^\circ \times 5^\circ$ (latitude/longitude). The problem with this method is that all of the backward trajectories begin at the receptor site and thus, the residence time is maximum in the cells surrounding the sampling location (Hopke et al., 2005). We refer to this effect as "central convergence". We have used a modification proposed by Poirot and Wishinski (1986) to avoid the geometrical "central convergence" effect and highlight the distant O_3 sources.

Backward trajectories have been also used to compute backward trajectory mean height (BTMH) plots. In this case BTMH plots represent the mean height of the air parcel when air masses passed above each $1^\circ \times 1^\circ$ cell.

2.4 Potential vorticity

Potential vorticity (PV; 1 PVU = $10^{-6}\,m^2\,s^{-1}\,K\,kg^{-1}$) analysis is a widely used tool to understand the STT exchange (e.g. Danielsen, 1968) since PV, the product of absolute vorticity and thermodynamic stability, is greater in the stratosphere than in the troposphere (Hoskins et al., 1985). The dynamical tropopause is typically defined with a PVU value ranging from 1 PVU (Shapiro et al., 1987) to 2 PVU (Appenzeller et al., 1996; Parrish et al., 2000). The dynamical tropopause is defined by (WMO) as the

ACPD
12, 28385–28450, 2012

1.6 PVU iso-surface. Therefore, it is assumed that tropospheric values of PVU > 1 are typical of tropospheric regions that have been impacted by stratospheric intrusions. Beekman et al. (1994) made use of the positive correlation of PV with O_3 in separating tropospheric O_3 sources on the basis of high and low PV. However, we should note that diabatic heating can reduce the PV values without changing O_3. So, PV must be viewed as a bottom-indicator of air masses with upper troposphere/lower stratosphere (UTLS) signature.

PV was obtained from ERA-Interim ECMWF (European Centre for Medium-Range Weather Forecasts) reanalysis. Daily reanalysis at 00:00, 06:00, 12:00 and 18:00 UTC were retrieved at 300, 400, 500, 600, 700, 775, 850 and 925 hPa levels from January 1988 to December 2009 in a regular grid with a spatial resolution of 0.5° latitude/longitude, within the geographical domain 20° N–50° W/70° N–30° E.

Maximum PV(PV_{max}) intercepted by daily 5-day backward trajectories for IZO was computed as follows: for each one of the 120 h of the backward trajectory the PV is calculated by performing a 3D nearest-neighbour interpolation with the 8-isobaric PV levels of the ECMWF reanalysis. PV was stored for each 1h point back of the back-trajectory. In this work we have used the PV_{max} found along each backward trajectory together with its latitude and longitude.

2.5 ^{7}Be and ^{210}Pb radiotracers

The ^{210}Pb radiotracer (half-life 22 yr) is the decay daughter of ^{222}Rn (half-life 3.8 days) which is emitted from soils (Turekian et al., 1977). So, ^{210}Pb is a tracer of air masses with continental boundary layer (CBL) signature (Balkanski et al., 1993). The ^{7}Be radiotracer (half-life 53.3 days) is produced by cosmic ray spallation reactions with nitrogen and oxygen in the stratosphere and upper troposphere (Viezee and Singh, 1980).

The ^{7}Be and ^{210}Pb radionuclides were measured at IZO on a daily basis within the AEROCE (AEROsol Ocean chemistry Experiment) project (Prospero et al., 1995), in the period 1989–1991, as tracers for upper troposphere/lower stratosphere (UTLS) and CBL air, respectively.

ACPD
12, 28385–28450, 2012

2.6 Carbon monoxide (CO)

Carbon monoxide (CO) is a good tracer of anthropogenic pollution because it has a relatively long lifetime in the FT, which permits the study of long range transport. Daily and hourly night-time CO averaged concentrations at IZO, corresponding to the period 2008–2011, have been used for the analysis of long-range transport of photochemical O_3 from polluted regions. CO concentrations have been obtained using an automated TEI 48C-TL (Thermo Electron Corporation) NDIR instrument. The NDIR system was calibrated every 3 months using a 10-ppm CO in N_2 standard from Air Liquide. Automatic zero checks and ambient air measurements are alternated in 15 min intervals to account for short-term drift. A Sofnocat 423 CO scrubber is used for the zero checks. The inlet filter is exchanged every 3 months. One-minute averages including additional instrument status information are stored. The NDIR system has been audited by the WCC-Ozone-CO-CH4-EMPA in 2009. This audit confirmed the stability and linearity of the instrument, and showed an error of about 10 % when compared to EMPA reference. However, continuous NDIR data have been corrected using discrete NOAA measurements of weekly samples collected in flasks. So, we expect an error lower than 10 %. CO data is used in this work to assess pollution long range transport by analyzing averaged daily O_3/CO ratios. So, the error associated to CO measurements is acceptable for our purposes.

2.6.1 PM_{10}

Daily nocturnal PM_{10} (particles less than 10 microns in diameter) concentrations at IZO in the period 2002–2009 have been used for assessing the impact of dust laden Saharan air masses on O_3 records. The PM_{10} measurement programme was described by Rodríguez et al. (2011).

ACPD
12, 28385–28450, 2012

2.6.2 North Atlantic Oscillation (NAO) index

The NAO is one of the major tele-connection patterns of the winter Northern Hemisphere (Wallace and Gutzler, 1981), and represents a measure of the strength of the westerlies across the North Atlantic. Monthly mean values of the NAO index have been obtained from NOAA Climate Prediction Center ftp://ftp.cpc.ncep.noaa.gov/wd52dg/data/indices/nao_index.tim. Indices are normalized using the 1981–2010 base period monthly means and standard deviations.

2.6.3 Tropospheric Ozone Residual (TOR)

Tropospheric Ozone Residual (TOR) data are measurements of tropospheric O_3 obtained by subtracting the stratospheric component of O_3 (in the stratospheric aerosol and gas experiment) from the total atmospheric column of O_3 (by use of the Total Ozone Measurement Spectrometer (TOMS) and Solar Backscattered Ultraviolet (SBUV) instruments from 1979–2000).

Data over the North Atlantic, Northern Africa and Europe, within the geographical domain 10° N–30° E/50° N–60° W, have been computed from the database available at NASA site: http://asd-www.larc.nasa.gov/TOR/data.html. A description of the technique can be found in Fishman and Balok (1999) and Fishman et al. (2003).

3 Results

3.1 Surface O_3 diurnal cycle

Large-scale subsidence, associated to the descending branch of the Hadley cell, is an important meteorological feature of the subtropical North Atlantic region. The quasi-permanent NNE trade winds flow over a relatively cold ocean surface that inhibits the development of convection in the MBL and enhances subsidence. A temperature inversion layer (TIL) separates two well differentiated air masses: the MBL and the FT (Font,

ACPD
12, 28385–28450, 2012

1956). The TIL is characterized by a layer of stratocumulus formed by condensation of water vapour onto the available pre-existing particles. The top of the TIL is generally located around 1200 m a.s.l. in summer and around 1800 m a.s.l. in winter. IZO normally lies above the TIL that traps local island pollutant emissions. However, under certain synoptic conditions, normally in winter, the TIL reaches the station level or, simply, the TIL is not observed. The effectiveness of the inversion in separating the MBL from the FT at IZO is reflected in the relative humidity typically > 60 % below the TIL and ~ 20 % above it. Diurnal variations in the altitudes of the bottom (1200 m during daylight and 900 m at night) and the top (1700 m during daylight and 1300 m at night) of the TIL are observed. The influence of buoyant airflows caused by the heating of the air located just above the terrain of the island is observed at IZO. This upslope effect is reflected in the daily cycle of CO_2 concentrations that shows lower values and higher standard deviations during daylight, due to uptake by vegetation growing at lower elevations on the slopes (Cuevas et al., 1992). During the night a catabatic air flow regime is well established over the station favouring the arrival of very clean air masses from higher levels.

The diurnal cycles of O_3 (Fig. 1) were obtained from the differences of O_3 for every hour compared with the night background level. The reference background level has been computed as follows. Firstly, the averages of the pre (00:00–07:00 h UTC) and post (21:00–00:00 h UTC) nights were computed. Then, the linear drift in time passing through both averages is used as the reference background level. The use of a linear drift allows for a background trend. Diurnal cycles of surface O_3 have been averaged for each month using hourly data for the entire period 1988–2009.

Surface O_3 diurnal variations show the lowest values during the afternoon due to an efficient dry deposition on very rough and dark volcanic mountain slopes covered with scattered bushes. This diurnal cycle is the opposite to that recorded in continental regions where a maximum during daylight is observed due to the photochemical production (e.g. Millán et al., 1997). The annual mean difference between the daily upslope and the nocturnal downslope surface O_3 values is within 2 ppbv in winter and autumn.

ACPD
12, 28385–28450, 2012

However, in summer and spring day-night differences are normally above 2 ppbv, being somewhat greater than 5 ppbv in June, and reaching up to 25 ppbv in some days. The amplitude and width of the diurnal O_3 "valley" is basically modulated by two factors: the solar radiation, and the consequent heating of the slopes surrounding the observatory, and the strength of the synoptic wind. In wintertime the heating of the slopes is minimal, and the strong synoptic winds dilute air masses from lower levels. By contrast, in spring and summer there is: (1) a strong warming of the soil (facilitating the mountain breeze); (2) the TIL associated to trade winds is recorded at its lowest level (around 800–1100 m a.s.l.), so the air flows from lower levels, where O_3 concentration is lower, and with a longer path available for dry deposition; and (3) the synoptic winds are usually very weak, resulting in a lower dilution of upslope air.

3.2 Annual and seasonal variations of surface O_3

Daily nocturnal (22:00–06:00 UTC) O_3 values, representative of subtropical FT conditions, have been analyzed for the entire record (1988–2009) using decomposition in three terms: inter-annual trend, annual cycle, and residual. A least squares fit of the daily data to the function:

$$f(t) = a_1 + a_2 t + a_3 t^2 + \sum_{i=1}^{p} [b_i \cos(w_i t) + c_i \sin(w_i t)] + \sum_{j=1}^{4} [d_j \cos(k_j) t + e_j \sin(k_j t)]$$

has been performed, where: t is the time in days ($t = 1$ for 1 January 1988); a_1, a_2, a_3, b_i and c_i are the parameters of the inter-annual trend to be determined; $p = 7$; d_j and e_j are the parameters of the annual cycle (which is assumed constant) to be determined; $w_i = 2\pi i/N$ with N equal to the number of days in the period 1988–2009 ($N = 8036$, number of valid data = 7790); $k_j = 2\pi j/T$ with $T = 365.25$ days. See Gómez-Peláez et al. (2006) for a detailed interpretation of this function. Note that in this work we have added a quadratic term in time, following Gómez-Peláez et al. (2012), in order to allow a non-periodic growth rate.

ACPD
12, 28385–28450, 2012

Figure 2 shows the inter-annual trend and the inter-annual trend + annual cycle. The average yearly mean O_3 value at IZO for the 22 yr period is 46.1 ppbv. The corresponding standard deviation of the mean is 0.12 ppbv. The root mean square of the residuals is 8.9 ppbv, and the peak-to-peak annual cycle amplitude is 15.4 ppbv. It is striking the O_3 increase observed between 1996 and 1998. There is a slight positive trend in the annual mean (0.09 ± 0.02 ppbv yr^{-1} or 0.19 ± 0.05 % yr^{-1}), that is slightly lower than at Mauna-Loa (0.37 ± 0.26 % yr^{-1}, Oltmans and Levy II, 1992). In European Alpine stations such as Sonnblick, Jungfraujoch, Hohenpeissenberg and Zugspitze trends are observed in the 0.1–0.4 % yr^{-1} range (Gilge et al., 2010). Over some Europeans stations (Hohenpeissenberg, Zugspitze and Mace Head) small trends or reductions during summer are observed, while there is an increase during winter (Oltmans et al., 2006). Mace Head, a site that is representative of O_3 changes in the air advected from the North Atlantic to Europe in the MBL, has shown a positive trend of 0.16 ± 0.04 ppb yr^{-1} over the entire period 1988–2007 but this positive trend has reduced during recent years (Tripathi et al., 2010). So, tropospheric O_3 trends over Europe do not show a homogeneous behaviour.

Long-term O_3 series should be analyzed by seasons since the processes of transport/production of surface O_3 and its precursors can be very different in each season. In Fig. 3 we have plotted the long-term surface O_3 P10th, P25th, P50th, P75th and P90th (1988–2009) for winter, spring, summer and autumn. Pnth is the n-percentile. In winter, a change (increase) in all percentiles is observed in 1997 with a maximum in 1999. A similar behavior is found in spring, but only in P50th, P75th and P90th with maximum values in 1998. The lower percentiles do not show significant changes. In summer the increase is smoothed, being only evident in higher percentiles (P75th and P90th). In autumn the change is observable from 1996 in percentiles $\geq$ P50th. Changes in percentile data series observed in the period 1996–1998 will be discussed in Sect. 4.

Figure 4a shows non detrended monthly means for surface O_3 at IZO. A broad maximum beginning in late spring (May), with frequent daily mean values of 60–70 ppbv, is observed. Rodríguez et al. (2004) compared the O_3 annual course at IZO with that

ACPD
12, 28385–28450, 2012

observed at Mauna-Loa, noting that in summer O_3 monthly means sharply decrease in the latter, while high O_3 events are frequent at IZO. The annual course is shifted towards high values (> P75th) in spring, mid values (P25th < P*n*th < P50th) in winter, and low values (< P25th) in autumn time, while summer contributes significantly in both low and high values (Fig. 4b). ND is the number of daily mean surface O_3 data in each percentile range for the total period 1988–2009. O_3 data above P90th are found in spring and summer whereas O_3 levels below P10th are found in late summer and autumn.

3.3 Synoptic climatology of surface O_3: transport pathways

A previous analysis of transport pathways of O_3 at IZO was performed by Rodríguez et al. (2004). In the present work we have incorporated a longer data series and followed a different approach, using the MCAR plots for each month for the entire surface O_3 data-set (Fig. 5). This methodology does not assume a priori geographical areas, and allows us to visualize the regions from which air masses reaching IZO come with different O_3 concentrations. Since at higher altitudes in the troposphere are expected higher concentrations of O_3, we have calculated the corresponding BTMH plots for each month of the year for the same period (Fig. 6).

Figure 5 shows in winter (January–March) a well-defined pattern with air masses coming from the North Atlantic and North America with a top-latitude located at about 60° N. It is also noticeable a latitudinal gradient with higher O_3 values in northern regions. Concerning the height of the backward trajectories (Fig. 6), a similar latitudinal distribution to the O_3 is observed, with higher altitudes to the north. The highest trajectory altitudes describe an arc-shape corridor from Western Europe to Northeast North America. Air masses with low O_3 coming from the Sahara are also recorded associated to very low height trajectories. In spring (April–June) we observe a similar O_3 pattern to winter, but with the following characteristics: (1) the latitudinal gradient is much higher, registering very high values at the northern edge of the cloud trajectories and Western Europe, describing an arch-shape pathway; (2) contributions from Sahara and southern part of the North Atlantic are lower; and (3) transport from North Amer-

ACPD
12, 28385–28450, 2012

ica, is defined much better in this season. The heights of backward trajectories (Fig. 6) show a similar pattern than in winter, although the lowest trajectories from Africa travel at higher altitudes. In summer months (July–September) there is a sharp change because basically only two geographical sectors of air mass pathways are identified: from North America, with associated medium and high O_3 values, and from the Sahara and Northern Sahel, with a lower latitude edge set at 10°–15° N, with low and very low O_3 values (Fig. 5). Air masses from North America and North Atlantic travel at relatively high altitude, whereas air masses from Sahara come from low levels (Fig. 6). It is noticeable the fact that trajectories from the Sahel, and those originated over North Africa and the Mediterranean Basin, travel at mid-high altitudes, mainly in July and August. In summertime the contribution from Western Europe is at its minimum, and the highest O_3 values describe an arc-shape pathway over the North Atlantic similar to that found in spring (Fig. 5). The O_3 and trajectory height patterns of autumn rapidly evolve to resemble those found in winter (Figs. 5 and 6), but with significantly lower O_3 values in the southern part of the trajectories cloud.

3.4 Low surface O_3 concentrations

The frequency distribution of trajectories by geographical sectors for low O_3 values (< P25th) registered at IZO is shown in Fig. 7a. Air masses that most often contribute to low levels of O_3 throughout the year are those from the subtropical North Atlantic (below 30° N). However, in summer, especially in July and August the Saharan air masses (with 60 % frequency) are the largest contributor to O_3 levels < P25th. There is a secondary maximum of African air masses in March, when dust layers occurring at low levels (usually within the MBL) impact IZO on their upper edge, although to a much lesser extent than in summer.

In winter, very low O_3 values are recorded also under fog conditions at IZO when the TIL is very high or simply it does not exist (normally with North Atlantic air masses). Hourly O_3 data shows a strong negative correlation with water vapour pressure (not shown here). In summer and autumn low O_3 levels are associated with the arrival of

ACPD
12, 28385–28450, 2012

North African air masses that originate from Southern Morocco, Western Sahara and Sahelian regions (25–35 % of occurrence frequency of values < P10th). These trajectories show low-level (< 1500 m) "start-points", which are usually associated with dust storms driven by surface local thermal lows over the Sahara (Prospero and Carlson, 1981).

There is a clear negative logarithmic relationship between PM_{10} and surface O_3 in all seasons for the period 2002–2009 (Fig. 8a). Surface O_3 daily nocturnal data have been grouped in 10 ppbv bin ranges from the minimum to maximum value. Each point of the plot represents the median value of surface O_3 concentrations associated to the mean value (and corresponding standard deviation of the mean) of PM_{10} in a determined bin range.

Most of the Saharan air masses have traveled within the African CBL and a high percentage of them correspond to lower levels (< 1500 m a.s.l.). A 67 % of the hourly PM_{10} records at IZO are lower than 10 $\mu g\,m^{-3}$ and monthly means of PM_{10} P75th are below 10 $\mu g\,m^{-3}$ through the year, except in summertime when significant PM_{10} concentrations are observed above P80th (26 $\mu g\,m^{-3}$).

Bonasoni et al. (2004) found also negative correlation between surface O_3 and coarse dust particles from North Africa at the high altitude Mt. Cimone station (North Italy). Andrey et al. (2010) found decreases of tropospheric O_3 up to 30 % in some layers, between 2 and 6 km altitude, during dust-laden Saharan air mass intrusions over Tenerife, compared to situations of non-Sahara air masses. This result agrees with the relationship between surface O_3 and PM_{10} found in this work.

The relationship between surface O_3 and ^{210}Pb is shown in Fig. 8b. There is not a clear relationship in winter, spring and autumn, probably due to the short variation range of ^{210}Pb values. However, in summer we obtain a logarithmic fit with a good correlation which resembles the O_3-PM_{10} fit in the same season. Prospero et al. (1995) had reported preliminary results of O_3-^{210}Pb relationship for summer-time.

The low O_3 values associated with African trajectories, might be due to a sum of all or some of the following causes: (1) air masses come from lower levels within the

ACPD
12, 28385–28450, 2012

Saharan CBL where O_3 concentrations are generally low (Güsten et al., 1996); (2) air masses originate from similar or lower latitudes which are not enriched with the latitudinal O_3 gradient existing in spring and summer in the Northern Hemisphere (London and Liu, 1992); (3) O_3 might be destroyed by dry deposition by suspended dust particles because of a larger surface area to dry deposition (Güsten et al., 1996); and (4) heterogeneous removal processes on dust aerosol by nitric acid (de Reus et al., 2000).

3.5 High surface O_3 concentrations

Figure 7b shows the monthly frequency of air masses that contribute most to O_3 values > P75th. Air masses from North America and oceanic sectors that have traveled over the North Atlantic are the largest contributors, by far, to high concentrations of O_3 at IZO. The highest daily O_3 values (> P90th) are observed in May and June, and in the first half of summer time (July and early August). Air mass residence times associated to O_3 concentrations between P75th and P90th (not shown here) show maximum values over Eastern United States (US) and North Atlantic between 30° and 55° N in winter, over the North Atlantic, from 25° to 55° N in spring, and near the Canary Islands and over North Western Africa in summer. In autumn the maximum residence times are much shorter and located to the northernmost position.

Summer-time is very interesting since O_3 records differ markedly from other seasons because the O_3 concentration undergoes large and rapid changes (Rodríguez et al., 2004), often from day-to-day. The alternation of dust transport from the Saharan CBL, lasting 3–7 days, with the arrival of air masses from high levels over the North Atlantic, modulated by the Azores anticyclone, account for these sudden changes in O_3 concentration.

3.6 Upper troposphere contribution

We have computed PV_{max} found by daily 5-day backward trajectories when intercepting ECMWF PV-reanalysis fields for each day of the period 1988–2009. We have observed

ACPD
12, 28385–28450, 2012

that mean values of PV_{max} in all seasons are slightly higher than 0.6 PVU. The average PV ranges approximately from 0.3 to 0.5 PVU in the low and middle troposphere (e.g. Rao et al., 2003), while 1 PVU is a typical value of the upper troposphere. So, it is noteworthy that in 10 % of days in winter and autumn, backward trajectories have been impacted by upper-troposphere air masses with PVU > 1.

Seasonal averages of PV_{max} values have been plotted for several surface O_3 bins (Fig. 9a), for winter, spring, summer and autumn. A fair O_3-PV_{max} correlation is found in all seasons with an O_3-PV_{max} slope $\sim 100\,ppbv\,PVU^{-1}$ for winter, spring and summer, and a slope slightly lower $\sim 53\,ppbv\,PVU^{-1}$, for autumn. These results emphasize the importance of air masses subsidence regardless of the origin of O_3 measured at IZO. Cooper et al. (2002) found over Western North Atlantic an O_3/PV ratio of $\sim 72\,ppbv\,PVU^{-1}$ in springtime and $\sim 42\,ppbv\,PVU^{-1}$ in late summer/early autumn. O_3/PV ratios found by Rao et al. (2003) at 500 hPa in Northern Europe range from 60 to 120 $ppbv\,PVU^{-1}$, which are of the same order as the O_3/PV_{max} ratios found at IZO.

Figure 10 shows the spatial distribution of averaged PV_{max} recorded by daily 5-day backward trajectories when they are crossed with the ECMWF PV-reanalysis fields for each season. Thresholds of 1 and 1.6 PVU are marked with black lines. PV_{max} maps provide an estimation of geographical regions of potential STT transport. PV_{max} might work as a meridional-height coordinate: the highest and most northerly the air mass travels, the more PV_{max} is associated. In Fig. 10 a latitudinal distribution, with much higher values of PV_{max} in the north, is clearly appreciated. In mid latitudes there is a belt with relatively high values between 45° N and 55° N that crosses the North Atlantic. This is consistent with the distribution of backward trajectory heights pattern (Fig. 6). In winter and spring this high PV_{max} belt coincides with the corridor where anthropogenic pollution is exported from North America to the North Atlantic (Cooper et al., 2002; Hegarty et al., 2009), as will be discussed later on. In summer PV_{max} values are substantially reduced. However, it is noticeable the relatively high PV_{max} values found in the vicinity of the Canary Islands over North Africa. This result is also

ACPD
12, 28385–28450, 2012

consistent with the high altitudes of backward trajectories observed over North Africa and the Mediterranean basin in July and August (Fig. 6).

The relationships between surface O_3 and ^{7}Be are shown in Fig. 9b for winter, spring, summer and autumn. The slope of O_3-^{7}Be best fit corresponding to winter is similar to the slope of O_3-^{7}Be best fit found by Dibb et al. (unpublished manuscript, 2006; www.espo.nasa.gov/docs/intex-na/Dibb_et_al_INTEXA.pdf) in mid and upper troposphere over North America during INTEX A flight experiment (1 mBq m^{-3} = 0.037 × fCi m^{-3}).

Li et al. (2002b) simulated ^{7}Be and ^{210}Pb concentrations at Tenerife for summertime and suggested that the positive O_3-^{7}Be and negative O_3-^{210}Pb correlation simply reflect the respective common vertical trends. However, Cuevas (1995) and Cuevas et al. (2000) reported some case analysis of high O_3 and high ^{7}Be data associated with air mass transport from the western part of cut-off lows (COLs) developed to the west of the Iberian Peninsula in spring and summer. Rodríguez et al. (2004) have also shown that episodes of O_3 > P90th at IZO are associated with strong subsidence in the FT at the western side of COLs located between the Canary Islands and the Iberian Peninsula. The STT processes are frequently associated to COL developments in the subtropical North Atlantic (Kentarchos et al., 2000). Cuevas and Rodríguez (2002), with an 11-yr climatology of ECMWF isentropic potential vorticity fields, concluded that the frequency of COLs and deep lows over the North Atlantic reach a maximum in May-July, in areas surrounding the Iberian Peninsula where these lows are more frequent. James et al. (2003), with a 15-yr climatology of STT exchange found similar results, concluding that the corridor parallel to the Atlantic coast of the Iberian Peninsula over the ocean down to the Canaries frequently receives stratospheric air.

Reiter et al. (1983) suggested a threshold value of 8 mBq m^{-3}, above which an air mass probably has stratospheric signature. We have estimated the impact on O_3 at IZO of air masses with daily mean values of ^{7}Be > 8 mBq m^{-3}. Results are summarized in Table 3. The percentage of cases per season with ^{7}Be > 8 mBq m^{-3} is significant in spring and summer (14.6 % and 8.9 % of cases/season, respectively), while in winter

ACPD
12, 28385–28450, 2012

and autumn the percentage of cases/season is much lower (3.8 % and 1.4 %, respectively). The impact of high ^{7}Be events on O_3 values at IZO is considerable, recording in these events O_3 averages that are 7 ppbv and 11 ppbv above O_3 climatological values (considering all days independently of ^{7}Be values) for spring and summer, respectively.

We have plotted the residence time of air masses with daily $^{7}Be > 8\,mBq\,m^{-3}$, for each season of the year, in Fig. 11. Higher residence times are observed in mid latitudes over northeast US extending over the North Atlantic in winter. In spring several maximum residence-times are observed over North Atlantic, but it is striking a maximum which extends along a north-south corridor over the Eastern North Atlantic stretching from Great Britain to the Canary Islands. Similar results were obtained by Rodríguez et al. (2004) for O_3 values within P50th–P100th in spring. In summer, the corridor is strengthened to the vicinity of the Canary Islands, and a secondary maximum is found in North Eastern North America extending over North Atlantic. In autumn this maximum is also identified, and some secondary high residence times near the Canary Islands are observed. In relation to the height at which air masses were travelling, it is noteworthy that in the spring and summer, they come from altitudes above 5 km. Summarizing, the source regions of high ^{7}Be air masses with maximum impact on O_3 at IZO are registered in a region around the Canaries extending to the north over North Atlantic in spring and summer. This region coincides with areas where COL developments and STT processes have been reported in previous studies (e.g. Cuevas and Rodríguez, 2002; James et al., 2003; Rodríguez et al., 2004). Nieto et al. (2005), from a 41-yr climatology of COLs in the Northern Hemisphere, reported three preferred areas of COLs occurrence, one of them being the Southern Europe and the Eastern Atlantic coast, in agreement with our results.

Recently, Hegarty et al. (2009) revealed that O_3 observations from TES (Tropospheric Emission Spectrometer) also evidence stratospheric intrusions associated with the cyclones over the North Atlantic. According to Wernli and Bourqui (2002), "deep exchange" denotes events where air parcels are rapidly transported from the stratosphere down to levels below 700 hPa level (deep-STT). The STT climatology from Sprenger

ACPD
12, 28385–28450, 2012

and Wernli (2003) shows that deep-STT is particularly strong in the 40°–65° N latitude band over the North Atlantic storm track region in winter, just in the high PV_{max} passageway we have found in winter (Fig. 10).

3.7 Relationship between O_3 and CO

Hegarty et al. (2009) reported that composites of O_3 and CO retrievals from TES sensor showed the main pollution export from North America extended in a band from 30° N to 45° N. Strong positive correlations between CO and surface O_3 are found in maritime stations off the coast of Canada (Kasibhatla et al., 1996). These positive correlations are attributed to the transport of photochemically generated O_3 from North America out over the North Atlantic (Parrish et al., 1993).

The concentration of CO at IZO shows a general increase during autumn and winter until the maximum is reached in late March, while the minimum is observed in middle August (Gómez-Peláez et al., 2012). The relationships between surface O_3 and CO at IZO, for each season of the year, are shown in Fig. 12. The good correlation between O_3 and CO at IZO in winter (with an O_3/CO slope of 0.94 ppbv ppbv^{-1}) and in spring when surface O_3 is within 30–50 ppbv and CO within 85–115 pbbv (with an O_3/CO slope of 0.91 ppbv ppbv^{-1}), supports the hypothesis of long-range transport of photochemically generated O_3 to IZO in these seasons, likely from North America according to the paths of the trajectories (Fig. 5). However, the lack of correlation between surface O_3 and CO found in summer and autumn suggests that O_3 enhancements are not directly caused by long-range transport of anthropogenic pollution in these seasons. These results agree with Li et al. (2002b) who found the strongest export of anthropogenic CO from North America in winter, and the weakest in summer.

Chin et al. (1994) found an O_3/CO slope $\sim$ 0.3 ppbv ppbv^{-1} in aged air masses at rural sites in Eastern North America. Hegarty et al. (2009) found that, under some meteorological conditions, some cyclones near the east coast of the US produced the greatest export to the lower FT with $O_3 > 65$ ppbv and a well-defined O_3-CO correlation

ACPD
12, 28385–28450, 2012

with an O_3/CO slope ~ 0.20 ppbv ppbv^{-1}, indicative of the overall impact of photochemical processes in North American continental export. However, Honrath et al. (2004) reported for the high mountain station of Pico in Azores, in the middle of the North Atlantic, that O_3 and CO were correlated during North American outflow events, with a slope averaging 1.0 ppbv ppbv^{-1}, more than 80 % larger than O_3/CO ratios observed in the Eastern US and near-shore outflow region. Honrath et al. (2004) explained these high ratios by the fact that air masses from North America outflow events have undergone days of photochemical processing, increasing the O_3/CO ratio.

The highest concentrations of CO at IZO (> 133 ppbv, above the P90th) are observed in winter and spring, mostly coming from North America (not shown here). In order to determine the impact of long-range transport of American pollution, and the origin of the fairly good O_3-CO correlation, we have analyzed the events in which, at least during five consecutive days, a good correlation ($r > 0.75$) between hourly concentrations of O_3 and CO is observed within the period 2008–2011. We have separated the events in four groups, according to O_3 ranges: > P75th (Type 1), P75th–P50th (Type 2), P50th–P25th (Type 3), and < P25th (Type 4). The O_3/CO ratios are summarized in Table 4. For O_3 within P75th–P100th range all the events meeting these criteria occurred in spring. These events presented the highest O_3/CO ratio (0.53 ± 0.09 ppbv ppbv^{-1}). For O_3 within P50th–P75th range the O_3/CO ratio was lower (0.42 ± 0.06 ppbv ppbv^{-1}), approximately half of the cases occurred during winter and the other half during spring. So, unambiguous transport of likely anthropogenic O_3 was observed and analyzed in winter and spring. In autumn long-range transport also takes place with lower O_3 concentrations, below P50th.

As demonstrated in Table 4, most of the events showing a good correlation between O_3 and CO are observed in spring and winter. Thus, a residence time analysis of air masses with an O_3-CO correlation > 0.75 has been performed for these two seasons (Fig. 13a). The results identify a main contribution from pollution episodes over North America in winter, with backward trajectories heights below 4 km, whereas in spring aged air masses (previously transported from North America) are found over North

ACPD
12, 28385–28450, 2012

Atlantic at high altitudes (above 4–5 km). In both cases maximum residence times are observed over Eastern US and Western North Atlantic, on a corridor bounded by the parallels 20° and 50° N. High trajectories suggest that pollution was injected previously over the US east coast, into the FT. These results agree with previous studies in which the warm conveyor belt associated with cyclonic pressure systems lift O_3 produced photochemically in the CBL up into the FT over eastern continental US and then the O_3 is transported by the westerlies across the North Atlantic onto Europe (Berkowtiz et al., 1996; Stohl and Trickl, 1999; Cooper and Parrish, 2004).

A 3-yr "climatology" of daily O_3/CO ratios is shown in Table 5. Mean (±standard deviation), median, P25th and P75th of O_3/CO ratios have been calculated for each season. In winter the O_3/CO ratios found during long-range transport events ($\sim 0.42\,\mathrm{ppbv\,ppbv^{-1}}$) agree quite well with the climatological ratio for this season. The ratios do not differ substantially from those calculated for high O_3 values (> P75th) and from those obtained for all values of O_3 for the study period. So, in winter, when the westerlies blow with their maximum intensity, O_3 measured at IZO might have a large contribution of pollution long-range transport from North America. The O_3/CO ratios reported near the pollution sources range from 0.2 to $0.3\,\mathrm{ppbv\,ppbv^{-1}}$ (e.g. Chin et al., 1994; Dickerson et al., 1995; Li et al., 2002b; Hegarty et al., 2009). The higher ratios found at IZO imply an additional O_3 amount and/or CO reduction which may arise, in part, from photochemical processing during transporting. In these conditions we could consider that the transport events labelled Type-2 (Table 4) correspond to "fresh pollution" that is transported rapidly from North America to the subtropical FT. In spring, the climatological O_3/CO ratios differ notably if we consider O_3 values > P75th ($\sim 0.58\,\mathrm{ppbv\,ppbv^{-1}}$) or all O_3 values ($\sim 0.47\,\mathrm{ppbv\,ppbv^{-1}}$). The average ratio found in pollution transport events labelled Type-1 ($\sim 0.53\,\mathrm{ppbv\,ppbv^{-1}}$) is between these two values. This may be due to the fact that in spring a higher insolation speeds up in-situ photochemistry in the FT (Yienger et al., 1999), and also to large-scale downward transport of O_3 rich air from the upper troposphere. So, O_3/CO ratios between 0.47 and $0.54\,\mathrm{ppbv\,ppbv^{-1}}$ might be typical of aged air masses originating in North Amer-

ACPD
12, 28385–28450, 2012

ica, while ratios above 0.54ppbv/ppbv might be explained by a mix of aged air masses and upper troposphere O_3 rich air masses. These assumptions are consistent with the analysis of residence times and heights of air masses characterized by high O_3-CO correlation (Fig. 13a). In spring, air masses come normally from higher altitudes than in winter, and the maximum of air masses residence-times is located northeast of the maximum found in winter, over western and central North Atlantic, further from pollution sources. On the other hand the seasonal averaged O_3/CO slopes (0.94 ppbv ppbv^{-1} for winter and 0.91 ppbv ppbv^{-1} for spring; see Fig. 12), which include all kinds of O_3 production and transport processes are higher than the O_3/CO ratios found in well identified long-range pollution transport (0.42–0.53 ppbv ppbv^{-1}), suggesting the contribution of a second source of O_3. The corridor of North American pollution events (Cooper et al., 2002; Hegarty et al., 2009) partially overlaps the belt with relatively high PV_{max} values found in winter and spring between 45° and 55° N, crossing the North Atlantic (Fig. 10). Differences found between the O_3/CO ratios at IZO and seasonal O_3/CO slopes, on one hand, and between the latter with O_3/CO ratios near the pollution sources, on the other hand, could be explained with the following conceptual model based on two processes: (1) O_3 continued to be produced in the plume during transporting in the FT (Honrath et al., 2004; Mao et al., 2006); and (2) contribution from the upper-level air transported downward in the descending dry airstream of cyclones over the North Atlantic, that may have enhanced the lower tropospheric O_3 keeping levels high (Hegarty et al., 2009). Bearing in mind that high O_3 values at IZO are normally associated to high altitude backward trajectories, high PV and high ^{7}Be values, this conceptual model might conciliate the apparently contradictory results of finding simultaneous positive O_3-CO correlation (Fig. 12), on the one hand, and positive O_3-PV (Fig. 9a) and O_3-^{7}Be (Fig. 9b) correlations, on the other hand, in winter and spring. So, a mixture of photochemical O_3 produced as a result of pollution export from North America and O_3 from stratospheric intrusions over the North Atlantic into the FT seems to be a likely process. This result agrees with Hegarty et al. (2009) who highlighted that some frequent meteorological patterns could produce a well-stirred region of the atmo-

ACPD
12, 28385–28450, 2012

sphere over the North Atlantic that continuously interleaves air masses originating from the lower mid- and upper troposphere, so favouring the mixing of polluted air masses with stratospheric O_3-rich air masses.

Concerning high O_3 values recorded at IZO in summer-time some authors (e.g. Schmitt and Carretero, 1992; Raes et al., 1997; Li et al., 2002b) hypothesized that, under some conditions during the summer, pollutants and photochemically-produced O_3 can be transported to the Canary Islands from the Iberian Peninsula and adjacent regions in Europe. Such conditions would be favoured by a coupled system consisting of the Iberian thermal low at ground level and anticyclonic subsidence aloft (Millán et al., 1997). However, this transport is most likely to occur within the MBL and not in the FT, as stated by Stohl et al. (2002) who analyzed the southward flow of European pollution in summer over the Mediterranean Basin and North Africa. The MCAR plots of O_3 pathways (Fig. 5) do not show significant transport of O_3 from Europe, and there is no relationship between O_3 and CO (Fig. 12). These results suggest a low probability of occurrence of pollution transport from Europe within the subtropical FT over the North Atlantic. These results agree with Duncan and Bey (2004) who concluded that there was no evidence of a summertime CO maximum at IZO in either the observations or the model simulations they performed for IZO. Concerning potential pollution from North America, Owen et al. (2006) documented that, on average, 38 % of the North American CO export occurs below 3 km altitude, and that advection of pollution layers at low levels, but decoupled from the BML, is responsible for the majority of transport to Central North Atlantic during summer-time. However, in summer, air masses arriving to IZO from the North Atlantic show a strong subsidence (see Fig. 6), traveling most of them at levels higher than 3 km. Moreover, aged air masses from North America that recirculate, turning around the Azores high anticyclonically (Auvray and Bey, 2005), are decoupled from the air mass pathways to IZO for the same reason. This may be the explanation for finding lower O_3/CO ratios at IZO than at the Azores Pico station.

The climatological O_3/CO ratios at IZO in summer-time are significantly higher, 0.56 ppbv ppbv^{-1} if we consider the whole dataset, and 0.71 ppbv ppbv^{-1} for O_3 >

ACPD
12, 28385–28450, 2012

P75th (the P75th O_3/CO ratio ~ 0.78 ppbv ppbv^{-1}). We have analyzed all the episodes in which O_3/CO ratio > 0.75 ppbv ppbv^{-1}. In these cases O_3 does not correlate with CO (O_3-CO correlation < 0.1). We have identified 41 cases in the period 2008–2011, 10 % of them in spring and 90 % in summer. The median value of the relative humidity associated to these events was 12 %, so very dry air suggesting a mid-upper-troposphere origin. The residence time analysis show two predominant origin of the air masses arriving at IZO (Fig. 13b): one located over North Africa and Central Mediterranean Basin, and the other one in a corridor stretching from the Canary Islands to the west of the Iberian Peninsula. These air masses come from altitudes higher than 4km showing a strong subsidence. All these events are associated with COL or deep lows developments which indicates they come from upper troposphere and likely could be influenced by STT processes. The geographical origin of these events agree with the PV_{max} distribution over North Africa (Fig. 10), and the maximum residence time distribution of air masses with $^7Be > 8$ mBq m^{-3} (Fig. 11). These results also agree with Nieto et al. (2005) who identified North Africa and the Mediterranean Basin (centred over the Italian Peninsula), and the corridor between the Canary Islands and the west of the Iberian Peninsula as main areas of occurrence of COLs in summer-time in the Northern Hemisphere.

3.8 The role of the NAO in tropospheric O_3 budget over the subtropical North Atlantic

The large swing in the phase of the NAO between 1995 and 1996 brought international attention to the physical connection between the NAO and e.g. availability of water in Scandinavia for hydropower generation (Hurrell et al., 2003). Indeed, changes in time series pattern have also been observed in surface O_3 records at IZO between 1996 and 1998 (Fig. 3). These changes cannot be attributed to changes in O_3 precursors, but to dynamical processes.

ACPD
12, 28385–28450, 2012

Positive phases of NAO indicate stronger Azores high and stronger Icelandic low and thus more active westerlies over the North Atlantic above 50° N. However, in lower mid latitudes and in the subtropical North Atlantic, winter positive phases of NAO mean less zonal west-to-east transport. Positive NAO also implies drier conditions than average over Northern Africa and a strong subtropical high pressure over the North Atlantic resulting in an increase of dust mobilization through strengthening of trade winds over the Sahara (Chiapello et al., 2005; Evan et al., 2006), and higher frequency of dust intrusions over the subtropical North Atlantic, and specifically over the Canaries (Alonso-Pérez et al., 2011). As we have shown in previous sections Saharan air masses loaded with mineral dust are associated with low concentrations of surface O_3 at IZO. The negative phase of NAO results in a higher flow of westerlies in the range 30°–45° N, as can be derived from the Dickson's scheme www.ices.dk/globec/data/bf4/naomap.htm.

Figure 14 shows the correlation between NAO and the zonal component of the wind (u) at 700 hPa (NCEP reanalysis) in winter, spring, summer and autumn for the entire period 1988–2009. A strong negative correlation is found in winter and autumn within the 20°–40° N belt, with a weaker correlation in spring. These results indicate a more effective air mass transport from North America to the Canaries within the low mid- and subtropical latitudes belt (between 20° and 40° N) with negative phase of NAO. So, this "transport belt" appears to be more active over the subtropical North Atlantic during negative phases of NAO in winter and spring. The effect of inter-continental transport is expected to be weaker in summer (Li et al., 2002a).

Hurrell et al. (2003) concluded that, generally, positive NAO phase winters are associated with a northeastward shift in the Atlantic storm activity. These results agree with findings of Andrade et al. (2008) who reported that the inter-annual correlation between the enlarged winter (October to March) NAO index and the total number of storms observed in the Azores Islands is negative and statistically significant. Sprenger and Wernli (2003) found that during the negative phase of NAO the low tropospheric destination of the deep-STT extends over a large region of the North Atlantic, below the 40° N parallel, covering the Canary Islands. Nieto et al. (2000) reported that during

ACPD
12, 28385–28450, 2012

positive NAO years, a high occurrence of COLs is detected for all the longitudes from 70° N to about 44° N, while during negative NAO years this high density of COLs is detected on a band from 60° N to 35° N over North Atlantic, so shifted southwards, and consequently, most likely to influence the subtropical region of the North Atlantic.

Creilson et al. (2003), using TOR data, found that the latitude band of greatest tropospheric O_3 was in the central mid latitudes (35°–40° N) and not the upper latitudes (40°–45° N). In Fig. 15 we have plotted the averaged TOR in winter (January–March) and spring (April–June) for years with NAO > +0.5 and for years with NAO < −0.5. It is noteworthy that in winter, a negative phase of NAO results in higher tropospheric O_3 amounts over the whole North Atlantic, mainly over 30° N. In spring, with a negative phase of NAO, there is a significant increase in tropospheric O_3 (∼ 10 %; 5 Dobson Units) in the band 20°–40° N, and especially in the longitude range between 40° W and 10° W, where the Canary Islands are situated. The relationship between TOR and NAO breaks down in summer and autumn when the westerlies are not so strong (Creilson et al., 2003). These results are confirmed by our analysis using surface O_3 at IZO (Table 6). In years with NAO < −0.5 surface O_3 is systematically higher than in years with NAO > +0.5 in all seasons. However, the highest differences between the two phases of NAO are observed in spring (∼ 3 ppbv), and the lowest in autumn (∼ 1 ppbv). The confidence level of O_3 differences is higher than 99 % for winter and spring.We can see in Fig. 16 that a significant change in air mass frequencies after 1996 is observed. For example, a considerable reduction in frequency of African air masses associated with O_3 < P25th, and a significant increase in frequency of air masses associated with O_3 > P75th from North America and North Atlantic are registered in winter at IZO. In winters with negative phases of NAO a more active jet stream and a higher frequency of storms over the North Atlantic, within the 30°–45° N belt, are observed, resulting in a stronger transport west-to-east of potentially polluted air masses from US and major impact of storms over this belt. This is a probable explanation to the sharp increase observed in the O_3 record between 1996 and 1998 (Fig. 3).

ACPD
12, 28385–28450, 2012

4 Summary/conclusions

A detailed analysis of a high quality long-term (22-yr) surface O_3 time series (1988–2009) at the subtropical high mountain IZO station has been conducted. Diurnal and seasonal O_3 variations have been assessed. Surface O_3 diurnal variations show the lowest values during the afternoon mainly due to an efficient dry deposition on the mountain slopes. The annual mean difference between the daily up-slope and the down-slope surface O_3 values ranges from 2 to 5 ppbv. The amplitude and width of the diurnal O_3 "valley" is basically modulated by two factors: the solar radiation, and the consequent heating of the slopes surrounding the Observatory, and the synoptic wind strength.

Daily nocturnal (22:00–06:00 UTC) O_3 values have been analyzed for the entire record. The average yearly mean O_3 value at IZO for the 22 yr period is 46.1 ppbv and the peak-to-peak annual cycle amplitude is 15.4 ppbv. There is a slight positive trend in the annual mean ($0.19 \pm 0.05\,\%\,yr^{-1}$ or $0.09\,ppbv\,yr^{-1}$). There is a notable increase in O_3 observed between 1996 and 1998. Seasonal O_3 cycles show a broad maximum beginning in late spring (May), with frequent daily means of 60–70 ppbv. The annual minimum is found in October with O_3 values often falling in the range 30–45 ppbv.

An analysis of the climatology of O_3 pathways using backward trajectories showed that higher O_3 values are associated with air masses travelling above 4 km altitude from North America and the North Atlantic Ocean, while low O_3 is transported from the Saharan CBL, largely corresponding to transport at lower altitudes (< 1500 m a.s.l.).

An extensive review of the potential O_3 production and transport processes into the FT of the North Atlantic subtropical region has been presented, incorporating other measurements from the IZO station such as PM_{10}, CO, ^{7}Be, ^{210}Pb, and additional information from backward trajectories and PV. A clear negative logarithmic relationship was observed between PM_{10} and surface O_3 for all seasons. A similar relationship was found between O_3 and ^{210}Pb, but only for summer.

ACPD
12, 28385–28450, 2012

A positive correlation between O_3 and PV_{max}, and between O_3 and ^7Be is found throughout the year, indicating that relatively high surface O_3 values at IZO originate from the middle troposphere and in some cases from the upper troposphere. Spatial analysis of PV_{max} show a belt with relatively high values between 45° and 55° N crossing the North Atlantic. In winter and spring this high PV_{max} belt coincides with the corridor where anthropogenic pollution is exported from North America to the North Atlantic. In summer the relatively high PV_{max} values found in the vicinity of the Canary Islands over North Africa are notable. The impact of high ^7Be events on O_3 values at IZO is considerable; O_3 averages recorded during these events are 7 ppbv and 11 ppbv above climatological values for spring and summer, respectively. Residence time analysis of air masses with daily $^7Be > 8\,mBq\,m^{-3}$ (threshold value above which an air mass has stratospheric signature) showed a region around the Canaries extending to the north over North Atlantic in spring and summer. This region coincides with areas where COL developments and STT processes have been reported in previous studies.

The influence of pollution long-range transport events on O_3 levels has been studied using CO data. At IZO a good correlation between O_3 and CO in winter (with an O_3/CO slope of $0.94\,ppbv\,ppbv^{-1}$) and in spring, when surface O_3 is within 30–50 ppbv and CO within 85–115 pbbv (with an O_3/CO slope of $0.91\,ppbv\,ppbv^{-1}$), is observed. This supports the hypothesis of long-range transport of photochemically generated O_3 from North America. In order to determine the impact of long-range transport of American pollution events, those days in which, at least during five consecutive days, a good correlation ($r > 0.75$) between hourly concentrations of O_3 and CO is observed within the period 2008–2011 were analyzed. These events presented the highest O_3/CO ratio ($0.53 \pm 0.09\,ppbv\,ppbv^{-1}$) in spring. For O_3 within P50th–P75th the O_3/CO ratio was lower ($0.42 \pm 0.06\,ppbv\,ppbv^{-1}$). Approximately half of the cases occurred during winter and the other half during spring. The time residence analysis highlights a main contribution from pollution episodes over North America in winter, whereas in spring the origin of the air masses are identified over North America as well over North Atlantic

ACPD
12, 28385–28450, 2012

at high altitudes. In winter the O_3/CO ratios ($\sim 0.42\,\mathrm{ppbv\,ppbv^{-1}}$) agree quite well with the climatological ratio for this season. So, in winter, when the westerlies blow with their maximum intensity, O_3 measured at IZO might be affected by pollution long-range transport from North America.

Differences found between the daily O_3/CO ratios at IZO and seasonal O_3/CO slopes and between the latter with O_3/CO ratios near the pollution sources could be explained with the following conceptual model based on two processes: (1) O_3 continued to be produced in the plume during its transport in the FT; and (2) contribution from the upper-level air transported downward in the descending dry airstream of cyclones over the North Atlantic, that may have enhanced the lower tropospheric O_3 keeping levels high. This conceptual model conciliates the apparently contradictory results of finding simultaneous positive O_3-CO correlation and positive O_3-PV_{max} and O_3-^{7}Be correlations in winter and spring. So, a mixture of photochemical O_3 produced as a result of pollution export from North America and "natural" O_3 from stratospheric intrusions over the North Atlantic into the FT seems to be a likely process. In summer the MCAR plots of O_3 pathways do not show significant transport of O_3 from Europe, and no relationship between O_3 and CO is also found. These results suggest a low probability of occurrence of pollution transport from Europe within the subtropical FT over the North Atlantic. We have analyzed all the episodes in which O_3/CO ratio $> 0.75\,\mathrm{ppbv\,ppbv^{-1}}$. In these cases, 10 % of them in spring and 90 % in summer, O_3 does not correlate with CO (O_3-CO correlation < 0.1).

The residence time analysis of air masses show two main origins: one located over North Africa and Central Mediterranean Basin, and the other one in a corridor stretching from the Canary Islands to the west of the Iberian Peninsula. These air masses come from altitudes higher than 4km and show a strong subsidence. All these events are associated with COL or deep lows developments which indicates they are caused by STT processes. The geographical origin of these events agree with the PV_{max} distribution over North Africa and the maximum residence time distribution of air masses with $^7\mathrm{Be} > 8\,\mathrm{mBq\,m^{-3}}$.

ACPD
12, 28385–28450, 2012

Taking into account all O_3-CO relationships found at IZO and in other studies, we propose the following approach concerning the origin of O_3 at IZO. Fresh Pollution O_3 from North America, mainly observed in winter, might be associated with O_3/CO ratios between ~ 0.34 and ~ 0.4 ppbv ppbv^{-1}. O_3/CO ratios within ~ 0.40–0.55 ppbv ppbv^{-1} range likely correspond to aged air masses originated in North America and North Atlantic, in winter, spring and autumn. Aged air masses in combination with inputs from the upper troposphere observed in spring, summer and autumn might be identified by O_3/CO ratios from ~ 0.55 to 0.62 ppbv ppbv^{-1}. In summer-time high O_3 values are associated with O_3/CO ratios > 0.65 ppbv ppbv^{-1}, normally the result of STT processes in regions neighbouring the Canary Islands (North Africa, and the corridor extending from Great Britain to the Canaries).

Summarizing, tropospheric O_3 recorded in the subtropical North Atlantic is the result of the interaction between transport of photochemical produced O_3 within the North American CBL, the in-situ photochemical O_3 produced within the FT during its transport over the North Atlantic, and the "natural" O_3 intrusions from the lower stratosphere over the North Atlantic and North Africa. However, we cannot discern the relative contribution of each main source quantitatively. For this, further studies are needed which might be supported with photochemical model simulations.

Finally, the role played by the NAO in the O_3 content over the North Atlantic, and specifically at IZO has been analyzed. The predominant high positive phase of NAO changes appreciably from 1995–1996. Since this date the NAO alternates between negative or neutral phases and positive phases. This change in the pattern of atmospheric circulation over the North Atlantic results in an increased flow of the westerlies in the mid-latitude and subtropical North Atlantic, thus favouring the transport of O_3 and its precursors from North America, and a higher frequency of storms over North Atlantic, with a likely higher incidence of STT exchange processes in mid latitudes. This resulted in an increase of tropospheric O_3 in the subtropical North Atlantic region after 1996 that has been reflected in surface O_3 records at IZO.

ACPD
12, 28385–28450, 2012

Averaged TOR data in winter for years with NAO < −0.5 shows higher tropospheric O_3 amounts over the whole North Atlantic, mainly over 30° N, compared to years with NAO > +0.5. In spring there is a significant increase in tropospheric O_3 in the band 20°–40° N, and especially in the longitude range between 40° W and 10° W, in the region of the Canaries, in years with negative phase of NAO. These results are confirmed by surface O_3 at IZO. Years with NAO < −0.5 show surface O_3 values systematically higher than those for years with NAO > +0.5. The highest differences between the two phases of NAO are observed in spring (∼ 3 ppbv), and the lowest in autumn (∼ 1 ppbv). This is an important issue in O_3 trend analysis since changes in the phase of the NAO could mask changes in emission of O_3 precursors that have occurred in the last twenty years. O_3 trends over the subtropical North Atlantic region must be properly interpreted taking into consideration phases of NAO. There is still considerable uncertainty in the prediction of NAO, but some studies suggest an intensification of the positive phase of NAO in a scenario of global warming (Gillett et al., 2003), which would impact on the content of tropospheric O_3 over the North Atlantic through the atmospheric mechanisms analyzed in this work.

Acknowledgements. This study has been developed within the GAW Programme at the Izaña Atmospheric Research Center, financed by AEMET. We are particularly grateful to the Izaña Observatory staff (www.aemet.izana.org) for carrying out carefully essential routine operations. We appreciate the accurate audits performed by the World Calibration Centre (WCC-Empa) for Surface Ozone, Carbon Monoxide, Methane and Carbon Dioxide, for providing a trustful and creditable O_3 and CO data quality assurance system at the Izaña Observatory. Data of radiotracers were obtained from the AEROCE project (Prof. Joseph Prospero as Principal Investigator). The authors would also like to express their gratitude to NOAA-ARL for the provision of the HYSPLIT transport and dispersion model (www.arl.noaa.gov/ready.html) used in this publication. PV data has been obtained from ERA-Interim ECMWF reanalysis. Monthly NAO index data have been obtained from NOAA/CPC. Zonal wind data-sets were retrieved from NCEP/NCAR reanalysis. TOR data have been computed from the database available at the NASA site http://asd-www.larc.nasa.gov/TOR/data.html.

ACPD
12, 28385–28450, 2012

References

Alonso-Pérez, S., Cuevas, E., Querol, X., Viana, M., and Guerra, J.: Impact of the Saharan dust outbreaks on the ambient levels of total suspended particles (TSP) in the marine boundary layer (MBL) of the Subtropical Eastern North Atlantic Ocean, Atmos. Environ., 41, 9468–9480, 2007. 28391

Alonso-Pérez, S., Cuevas, E., Pérez, C., Querol, X., Baldasano, J., Draxler, R., and de Bustos, J.: Trend changes of African airmass intrusions in the marine boundary layer over the subtropical Eastern North Atlantic region in winter, Tellus B, 63B, 255–265, 2011. 28412

Andrade, C., Trigo, R., Freitas, M., Gallego, M., Borges, P., and Ramos, A.: Comparing historic records of storm frequency and the North Atlantic Oscillation (NAO) chronology for the Azores region, The Holocene, 18, 745–754, 2008. 28412

Andrey, J., Gil, M., Alonso-Pérez, S., Parrondo, C., Redondas, A., and Cuevas, E.: Tropospheric ozone under Saharan dust: a statistical study on vertical distribution, in: International Aerosol Conference, number 873, Helsinki (Finland), 29 August–3 September, 2010. 28401

Appenzeller, C., Davies, H., and Norton, W.: Fragmentation of stratospheric intrusions, J. Geophys. Res., 101, 1435–1456, 1996. 28392

Appenzeller, C., Weiss, A., and Staehelin, J.: North Atlantic oscillation modulates total ozone winter trends, Geophys. Res. Lett., 27, 1131–1134, 2000. 28388

Auvray, M. and Bey, I.: Long-range transport to Europe: seasonal variations and implications for the European ozone budget, Geophys. Res. Lett., 110, D11303, 1–22, doi:10.1029/2004JD005503, 2005. 28410

Balkanski, Y. J., Jacob, D., Gardner, G., Graustein, W., and Turekian, K.: Transport and residence times of tropospheric aerosols inferred from a global three-dimensional simulation of ^{210}Pb, J. Geophys. Res., 98, 20573–20586, 1993. 28393

Beekman, M., Ancellet, G., and Megie, G.: Climatology of tropospheric ozone in southern Europe and its relation to potential vorticity, J. Geophys. Res., 99, 12841–12853, 1994. 28393

Berkowtiz, C., Daum, P., Spicer, C., and Busness, K.: Synoptic patterns associated with the flux of excess ozone to the western North Atlantic, J. Geophys. Res., 101, 28923–28933, 1996. 28408

Bonasoni, P., Cristofanelli, P., Calzolari, F., Bonafè, U., Evangelisti, F., Stohl, A., Zauli Sajani, S., van Dingenen, R., Colombo, T., and Balkanski, Y.: Aerosol-ozone correlations during

ACPD
12, 28385–28450, 2012

dust transport episodes, Atmos. Chem. Phys., 4, 1201–1215, doi:10.5194/acp-4-1201-2004, 2004. 28401

Chiapello, I., Moulin, C., and Prospero, J.: Understanding the long-term variability of African dust transport across the Atlantic as recorded in both Barbados surface concentrations and large-scale Total ozone Mapping Spectrometer (TOMS) optical thickness, J. Geophys. Res., 110, D18S10, doi:10.1029/2004JD005132, 2005. 28412

Chin, M., Jacob, D., Munger, J., Parrish, D. D., and Doddridge, B.: Relationship of ozone and carbon monoxide over North America, J. Geophys. Res., 99, 14565–14573, doi:10.1029/2004JD005132, 1994. 28406, 28408

Cooper, O. and Parrish, D.: Air Pollution Export from and Emport to North America: Experimental Evidence, The Handbook of Environmental Chemistry, vol. 4G, Springer, New York, 2004. 28408

Cooper, O., Moody, J., Parrish, D., Trainer, M., Holloway, J., Ryerson, T., Hüler, G., Fehsenfeld, F., Oltmans, S., Evans, M., and Evans, M. J.: Air Pollution Export from and Emport to North America: Experimental Evidence, vol. 4G, Springer, New York, 2002. 28403, 28409

Creilson, J. K., Fishman, J., and Wozniak, A. E.: Intercontinental transport of tropospheric ozone: a study of its seasonal variability across the North Atlantic utilizing tropospheric ozone residuals and its relationship to the North Atlantic Oscillation, Atmos. Chem. Phys., 3, 2053–2066, doi:10.5194/acp-3-2053-2003, 2003. 28387, 28413

Cuevas, E.: Estudio del Comportamiento del Ozono Troposférico en el Observatorio de Izaña (Tenerife) y su Relación con la Dinámica Atmosférica, Ph. D. thesis, Facultad de Ciencias Físicas, Universidad Complutense de Madrid, 1995. 28404

Cuevas, E. and Rodríguez, J.: Statistics of cutoff lows over the North Atlantic (in Spanish), in: Proceedings Tercera Asamblea Hispano-Portuguesa de Geodesia y Geofisica, Valencia, Spain, 4-8 February, 2002, 1-3, Comision Española de Geodesia y Geofisica, Edited by Editorial UPV, Valencia, Spain, 2002. 28404, 28405

Cuevas, E., Díaz, A., and Martín, F.: Atmospheric Carbon Dioxide Concentration at Izaña BAPMoN Observatory, Canary Islands, 1984–1990, in: Proceedings 19th ITM on Air Pollution Modeling and its Applications, NATO/CCMS, Ierapetra, Greece, 29 September–4 October 1991, 45–46, edited by: van Dop, H. and Kallos, G., Plenum Press, New York, USA, 1992. 28396

Cuevas, E., Diamantino, V., and Sancho, J.: Stratosphere-Troposphere Exchange events over North Atlantic subtropical region, in: Proc. Second Asamblea Hispano Portuguesa de Geode-

ACPD

12, 28385–28450, 2012

sia y Geofisica, edited by Instituto Geofisico do Infante D. Luis (Portugal), S11-16, pp. 451–452, Lagos (Portugal), 8–12 February, 2000. 28404
Danielsen, E.: Stratospheric-tropospheric exchange based on radioactivity ozone and potential vorticity, J. Atmos. Sci., 25, 502–518, 1968. 28387, 28392
de Reus, M., Dentener, F., Thomas, A., Borrmann, S. J. S., and Lelieveld, J.: Airborne observations of dust aerosol over the North Atlantic Ocean during ACE 2 – indications for heterogeneous ozone destruction, J. Geophys. Res., 105, 15263–15275, doi:10.1029/2000JD900164, 2000. 28402
Dickerson, R., Doddridge, B., Kelley, P., and Rhoads, K.: Large scale pollution of the atmosphere over the remote Atlantic Ocean: evidence from Bermuda, J. Geophys. Res., 10, 8945–8952, 1995. 28408
Draxler, R. and Rolph, G.: HYSPLIT (Hybrid Single-Particle Lagrangian Integrated Trajectory) Model access via NOAA ARL READY, Tech. rep., NOAA Air Resources Laboratory, Silver Spring, MD, available at: http://www.arl.noaa.gov/ready/hysplit4.html,(last access: March 2012), 2003. 28391
Duncan, B. N. and Bey, I.: A modeling study of the export pathways of pollution from Europe: seasonal and interannual variations (1987–1997), J. Geophys. Res., 109, D08301, doi:10.1029/2003JD004079, 2004. 28388, 28410
Eckhardt, S., Stohl, A., Beirle, S., Spichtinger, N., James, P., Forster, C., Junker, C., Wagner, T., Platt, U., and Jennings, S. G.: The North Atlantic Oscillation controls air pollution transport to the Arctic, Atmos. Chem. Phys., 3, 1769–1778, doi:10.5194/acp-3-1769-2003, 2003. 28388
Evan, A. T., Heidinger, A. K., and Knippertz, P.: Analysis of winter dust activity off the coast of West Africa using a new 24-year over-water advanced very high resolution radiometer satellite dust climatology, J. Geophys. Res., 111, D12210, doi:10.1029/2005JD006336, 2006. 28412
Fishman, J. and Balok, A. E.: Calculation of daily tropospheric ozone residuals using TOMS and empirically improved SBUV measurements: application to an ozone pollution episode over the Eastern United States, J. Geophys. Res., 104, 30319–30340, 1999. 28395
Fishman, J. and Crutzen, P.: The Origin of ozone in the troposphere, Nature, 274, 855–858, 1978. 28387
Fishman, J., Wozniak, A. E., and Creilson, J. K.: Global distribution of tropospheric ozone from satellite measurements using the empirically corrected tropospheric ozone residual tech-

ACPD
12, 28385–28450, 2012

nique: Identification of the regional aspects of air pollution, Atmos. Chem. Phys., 3, 893–907, doi:10.5194/acp-3-893-2003, 2003. 28395
Font, I.: El Tiempo Atmosférico de las Islas Canarias, Servicio Meteorológico Nacional, Serie A, no. 26, INM, Madrid, 1956. 28395
Gilge, S., Plass-Duelmer, C., Fricke, W., Kaiser, A., Ries, L., Buchmann, B., and Steinbacher, M.: Ozone, carbon monoxide and nitrogen oxides time series at four alpine GAW mountain stations in central Europe, Atmos. Chem. Phys., 10, 12295–12316, doi:10.5194/acp-10-12295-2010, 2010. 28388, 28398
Gillett, N., Graf, H., and Osborn, T. J.: The North Atlantic Oscillation: climatic significance and environmental impact, in: Geophys. Monogr. Ser., edited by: Hurrell, J., Kushnir, Y, Ottersen, G. and Visbeck, M., vol. 134, AGU, Washington, D. C., 193–210, 2003. 28418
Gómez-Peláez, A., Ramos, R., and Pérez-delaPuerta, J.: Methane and Carbon Dioxide Continuous Measurements at Izaña GAW station (Spain), in: 13th WMO/IAEA Meeting Experts on Carbon Dioxide, other Greenhouse gases, and Related Tracer Measurements Techniques, edited by: Miller, J., World Meteorological Organization (TD No.1359), Boulder, Colorado, USA, 19-22 September, 2005, World Meteorological Organization, 180–184, 2006. 28397
Gómez-Peláez, A., Ramos, R., Gómez-Trueba, V., Novelli, P., and Campo-Hernandez, R.: A statistical approach to quantify uncertainty in carbon monoxide measurements at the Izaña global GAW station: 2008–2011, Atmos. Meas. Tech. Discuss., 5, 6949–6989, doi:10.5194/amtd-5-6949-2012, 2012. 28397, 28406
Graustein, W. and Turekian, K.: ^{7}Be and ^{210}Pb indicate an upper troposphere source for elevated ozone in the summertime subtropical free troposphere of the Eastern North Atlantic, Geophys. Res. Lett., 23, 539–542, 1996. 28387
Güsten, H., Heinrich, G., Mönnich, E., Sprung, D., Weppner, J., Ramadan, A. B., Ezz El-Din, M. R. M., Ahmed, D. M., and Hassan, G. K. Y.: On-line measurements of ozone surface fluxes, II, surface level ozone fluxes onto the Sahara desert, Atmos. Environ., 30, 911–918, 1996. 28402
Hegarty, J., Mao, H., and Talbot, R.: Synoptic influences on springtime tropospheric O3 and CO over the North American export region observed by TES, Atmos. Chem. Phys., 9, 3755–3776, doi:10.5194/acp-9-3755-2009, 2009. 28387, 28403, 28405, 28406, 28408, 28409
Honrath, R. E., Owen, R. C., and Val Martin, M. E. A.: Regional and hemispheric impacts of anthropogenic and biomass burning emissions on summertime CO and ozone in the North At-

ACPD
12, 28385–28450, 2012

lantic lower free troposphere, J. Geophys. Res., 109, D24310, doi:10.1029/2004JD005147, 2004. 28407, 28409
Hopke, P., Zhou, L., and Poirot, R.: Reconciling trajectory ensemble receptor model results with emissions, Environ. Sci. Technol., 39, 7980–7983, 2005. 28392
Hoskins, B. J., McIntyre, M., and Robertosn, A.: On the use and significance of isentropic potential vorticity maps, Q. J. Roy. Meteorol. Soc., 111, 877–946, 1985. 28392
Hurrell, J., Kushnir, Y., Ottersen, G., and Visbeck, M.: The North Atlantic Oscillation: Climate Significance and Environmental Impact, Geophysical Monograph Series, 134, American Geophysical Union, Washington DC, USA, 2003. 28411, 28412
James, P., Stohl, A., Foster, C., Eckhard, S., Seibert, P., and Frank, A.: A 15-years climatology of stratosphere-troposphere exchange with a Lagrangian particle dispersion model: 2. Mean climate and seasonal variability, J. Geophys. Res., 108, 8522, doi:10.1029/2002JD002636, 2003. 28387, 28404, 28405
Jonson, J. E., Simpson, D., Fagerli, H., and Solberg, S.: Can we explain the trends in European ozone levels?, Atmos. Chem. Phys., 6, 51–66, doi:10.5194/acp-6-51-2006, 2006. 28387, 28388, 28389
Junge, C.: Global ozone budget and exchange between stratosphere and troposphere, Tellus, 14, 363–377, 1962. 28387
Kasibhatla, P., Levy II, H., Klonecki, A., and Chameides, W. L.: Three-dimensional view of the large-scale tropospheric ozone distribution over the North Atlantic Ocean during summer, J. Geophys. Res., 101, 29305–29316, 1996. 28406
Kentarchos, A., Roelofs, G., Lelievel, J., and Cuevas, E.: On the origin of elevated surface ozone concentrations at Izaña Observatory, Tenerife during late March 1996, Geophys. Res. Lett., 27, 3699–3702, 2000. 28404
Lelieveld, J. and Dentener, F.: What controls tropospheric ozone?, J. Geophys. Res., 105, 3531–3551, 2000. 28387
Levy, H. I.: Normal atmosphere: large radical and formaldehyde concentrations predicted, Science, 173, 141–143, 1971. 28387
Levy, H. I., Mahlman, J., Moxim, W., and Liu, S.: Tropospheric ozone: the role of transport, J. Geophys. Res., 90, 3753–3772, 1985. 28387
Li, Q., Jacob, D., Bey, I., Palmer, P., Duncan, B. N., Field, B. D., Martin, R. V., Fiore, A. M., Yantosca, R. M., Parrish, D. D., Simmonds, P. G., and Oltmans, S.: Transatlantic transport of

ACPD
12, 28385–28450, 2012

pollution and its effects on surface ozone in Europe and North America, J. Geophys. Res., 107, 4166, doi:10.1029/2001JD001422, 2002a. 28387, 28412
Li, Q., Jacob, D., Fairlie, T., Liu, H., Yantosca, R., and Martin, R.: Stratospheric versus pollution influences on ozone at Bermuda: reconciling past analyses, J. Geophys. Res., 107, 4611, doi:10.1029/2002JD002138, 2002b. 28404, 28406, 28408, 28410
Logan, J.: Tropospheric ozone: seasonal behavior, trends, and antropogenic influence, J. Geophys. Res., 90, 10463–10482, 1985. 28387
London, J. and Liu, S.: Long-term tropospheric and lower stratospheric ozone variations from ozonesonde observations, J. Atmos. Terr. Phys., 54, 599–625, 1992. 28402
Mao, H., Talbot, R., Troop, D., Johnson, R., Businger, S., and Thompson, A. M.: Smart balloon observations over the North Atlantic: ozone data analysis and modeling, J. Geophys. Res., 111, 599–625, doi:10.1029/2005JD006507, 2006. 28409
Millán, M., Salvador, R., Mantilla, E., and Kallos, G.: Photo-oxidant dynamics in the Mediterranean Basin in summer: results from European research projects, J. Geophys. Res., 102, 8811–8823, 1997. 28396, 28410
Mitchel, J.: The greenhouse effect and climate change, Rev. Geophys., 27, 115–139, 1989. 28387
Moody, J. L., Davenport, J. C., Merrill, J. T., Oltmans, S. J., Parrish, D. D., Holloway, J. S., Levy II, H., Forbes, G. L., Trainer, M., and Buhr, M.: Meteorological mechanisms for transporting ozone over the western North Atlantic Ocean: a case study for August 24–29, J. Geophys. Res., 101, 29213–29227, 1996. 28387
Nieto, R., Gimeno, L., Ribera, P., Gallego, D., García, R., and Hernández, E.: Effects of the North Atlantic Oscillation on the spatial distribution of cut-off low (COL) systems in the Northern Hemisphere, in: Proceedings of the AGU Chapman Conference "The North Atlantic Oscillation", Vigo, Spain, 28 November–1 December, available at: http://xtide.ldeo.columbia.edu/~visbeck/nao/poster/, (last access: October, 2012), 2000. 28412
Nieto, R., Gimeno, L., de la Torre, L., Ribera, P., Gallego, D., García-Herrera, R., García, J., Núñez, M., Redaño, A., and Lorente, J.: Climatological features of cut-off low systems in the Northern Hemisphere, J. Climate, 18, 3085–3103, 2005. 28405, 28411
Oltmans, S. and Levy II, H.: Seasonal cycle of surface ozone over the Western North Atlantic, Nature, 358, 392–394, 1992. 28398
Oltmans, S., Levy II, H., Harris, J., Merrill, J., Moody, J., Lathrop, J., Cuevas, E., Trainer, M., O'Neill, M., Prospero, J., Vömel, H., and Johnson, B.: Summer and spring ozone profiles

ACPD
12, 28385–28450, 2012

over the North Atlantic from ozonesonde measurements, J. Geophys. Res., 101, 29179–29200, 1996. 28387

Oltmans, S., Lefohn, A., Harris, J., Galbally, I., Scheel, H., Bodeker, G., Brunke, E., Claude, H., Tarasick, D., Johnson, B., Simmonds, P., Shadwick, D., Anlauf, K., Hayden, K., Schmidlin, F., Fujimoto, T., Akagi, K., Meyer, C., Nichol, S., Davies, J., Redondas, A., and Cuevas, E.: Long-term changes in tropospheric ozone, Atmos. Environ., 40, 3156–3173, 2006. 28388, 28398

Ordóñez, C., Brunner, D., Staehelin, J., Hadjinicolaou, P., Pyle, J., Jonas, M., Wernli, H., and Prevot, A. S. H.: Strong influence of lowermost stratospheric ozone on lower tropospheric background ozone changes over Europe, Geophys. Res. Lett., 34, L07805, doi:10.1029/2006GL029113, 2007. 28388

Owen, R. C., Cooper, O. R., Stohl, A., and Honrath, R. E.: An analysis of the mechanisms of North American pollutant transport to the Central North Atlantic lower free troposphere, J. Geophys. Res., 111, D23S58, doi:10.1029/2006JD007062, 2006. 28410

Parrish, D., Holloway, J. S., Trainer, M., Murphy, P., Forbes, G., and Fehsenfeld, F.: Export of North American ozone pollution to the North Atlantic Ocean, Science, 259, 1436–1439, doi:10.1126/science.259.5100.1436, 1993. 28387, 28406

Parrish, D. D., Holloway, J. S., and Jakoubek, R. E. A.: Mixing of anthropogenic pollution with stratospheric ozone: a case study from the North Atlantic wintertime troposphere, J. Geophys. Res., 105, 24363–24374, 2000. 28392

Poirot, R. and Wishinski, P.: Visibility, sulphate and air mass history associated with the summertime aerosol in Northern Vermont, Atmos. Environ., 20, 1457–1469, 1986. 28392

Prather, M., Gauss, M., and Berntsen, T. E. A.: Fresh air in the 21st century?, Geophys. Res. Lett., 30, 1100, doi:10.1029/2002GL016285, 2003. 28387

Prospero, J. and Carlson, T.: Saharan air outbreaks over the tropical North Atlantic, Pageoph., 119, 677–691, doi:10.1029/2002GL016285, 1981. 28401

Prospero, J., Schmitt, R., Cuevas, E., Savoie, D., Graustein, W., Turekian, K., Volz-Thomas, A., Díaz, A., Oltmans, S., and Levy, H.: Temporal variability of ozone and aerosols in the free troposphere over the Eastern North Atlantic, Geophys. Res. Letts., 22, 2925–2928, 1995. 28393, 28401

Raes, F., VanDingenen, R., Cuevas, E., VanVelthoven, P. F. J., and Prospero, J. M.: Observations of aerosols in the free troposphere and marine boundary layer of the subtropical

ACPD
12, 28385–28450, 2012

Northeast Atlantic: discussion of processes determining their size distribution, J. Geophys. Res., 102, 21315–21328, 1997. 28410
Ramanathan, V., Cicerone, R., Singh, H. B., and Kiehl, J.: Trace gas trends and their potential role in climate change, J. Geophys. Res., 90, 5547–566, 1985. 28387
Rao, T. N., Kirkwood, S., Arvelius, J., von der Gathen, P., and Kivi, R.: Climatology of UTLS ozone and the ratio of ozone and potential vorticity over northern Europe, J. Geophys. Res., 108, 4703, doi:10.1029/2003JD003860, 2003. 28403
Reiter, R., Munzert, K., Kanter, H., and Poetzl, K.: Cosmogenic radionuclides and ozone at a mountain station at 3.0 km a.s.l., Tech. Rep., Arc. Met. Geoph.Biocl., Ser. B, 32, 131–160, Garmisch-Partenkirchen, Germany, doi:10.1007/BF02273971, 1983. 28404
Rodríguez, S., Torres, C., Guerra, J., and Cuevas, E.: Transport pathways of ozone to marine and free-troposphere sites in Tenerife, Canary Islands, Atmos. Environ., 38, 4733–4747, 2004. 28398, 28399, 28402, 28404, 28405
Rodríguez, S., Alastuey, A., Alonso-Pérez, S., Querol, X., Cuevas, E., Abreu-Afonso, J., Viana, M., Pérez, N., Pandolfi, M., and de la Rosa, J.: Transport of desert dust mixed with North African industrial pollutants in the subtropical Saharan Air Layer, Atmos. Chem. Phys., 11, 6663–6685, doi:10.5194/acp-11-6663-2011, 2011. 28392, 28394
Rolph, G.: Real-time Environmental Applications and Display System (READY), Tech. rep., NOAA Air Resources Laboratory, Silver Spring, M. D., available at: http://www.arl.noaa.gov/ready/hysplit4.html, (last access: September 2012), 1983. 28391
Scheel, H.-E.: Ozone climatology studies for the Zugspitze and neighboring sites in the German Alps, edited by: Lindskog, A., TOR-2 Final Report, EUROTRAC-2 ISS, 134–139, GSF Research Center, Munich, Germany, 1983. 28388
Schmitt, R. and Carretero, P.: Ozone in the Free Troposphere Over The North Atlantic: Production and Long-Range Transport, edited by Hov,Ø., EUROTRAC-2, German Research Center for Environmental Health (GmbH), Munich, Germany, 1992. 28410
Shapiro, M., Hampel, T., and Krueger, A.: The arctic tropopause fold, Mon. Weather Rev., 115, 444–454, 1987. 28392
Solomon, S., Qin, D., Manning, M., Chen, Z., Marquis, M., Averyt, K., Tignor, M., and Miller, H. (eds.): IPCC AR4 WG1, Climate Change 2007: The Physical Science Basis, Contribution of Working Group I to the Fourth Assessment Report of the Intergovernmental Panel on Climate Change, Cambridge University Press, Cambridge, UK and New York, NY, USA, 2007. 28388

ACPD
12, 28385–28450, 2012

Sprenger, M. and Wernli, H.: A northern hemispheric climatology of cross-tropopause exchange for the ERA15 time period (1979–1993), J. Geophys. Res., 108, 8521, doi:10.1029/2002JD002636, 2003. 28405, 28412

Staehelin, J. and Poberaj, C.: Long-term Tropospheric ozone Trends: a Critical Review, vol. 33, Advances in Global Change Research, Climate Variability and Extremes during the Past 100 Years, IV, edited by: Bronniman, S., Luterbacher, J., Ewen, T., Diaz, H, Stolarski, R., Neu, U., Springer, Geneva, Switzerland, 2008. 28388

Stohl, A.: A 1-year Lagrangian "climatology" of airstreams in the Northern Hemisphere troposphere and lowermost stratosphere, J. Geophys. Res., 106, 7263–7279, 2001. 28387

Stohl, A. and Trickl, T.: A textbook example of long-range transport: simultaneous observation of ozone maxima of stratospheric and North American origin in the free troposphere over Europe, J. Geophys. Res., 104, 30445–30462, 1999. 28408

Stohl, A., Eckhardt, S., Forster, C., James, P., and Spichtinger, N.: On the pathways and timescales of intercontinental air pollution transport, J. Geophys. Res., 107, 4684, doi:10.1029/2001JD001396, 2002. 28387, 28410

Tarasova, O., Elansky, N., Kuznetsov, G., Kuznetsova, I., and Senik, I.: Impact of air transport on seasonal variations and trends of surface ozone at Kislovodsk High Mountain stations, J. Atmos. Chem., 45, 245–259, doi:10.1029/2002JD002636, 2003. 28388

Tarasova, O. A., Senik, I. A., Sosonkin, M. G., Cui, J., Staehelin, J., and Prévôt, A. S. H.: Surface ozone at the Caucasian site Kislovodsk High Mountain Station and the Swiss Alpine site Jungfraujoch: data analysis and trends (1990–2006), Atmos. Chem. Phys., 9, 4157–4175, doi:10.5194/acp-9-4157-2009, 2009. 28388

Thompson, A.: The oxidizing capacity of the Earth's atmosphere: probable past and future changes, Science, 256, 1157–1165, 1992. 28387

Tiao, G., Box, G., and Hamming, W.: Analysis of Los Angeles photochemical smog data: a statistical overview, J. Air Poll. Control Assoc., 25, 260–268, 1975. 28387

Tripathi, O. P., Jennings, S. G., O'Dowd, C. D., Coleman, L., Leinert, S., O'Leary, B., Moran, E., O'Doherty, S., and Spain, T. G.: Statistical analysis of eight surface ozone measurement series for various sites in Ireland, J. Geophys. Res., 115, 85–89, doi:10.1029/2010JD014040, 2010. 28398

Turekian, K. K., Nozaki, Y., and Benninger, L. K.: Geochemistry of atmospheric radon and radon products, Annu. Rev. Earth Planet. Sci., 5, 227–255, 1977. 28393

ACPD

12, 28385–28450, 2012

Val Martin, M., Honrath, R. E., Owen, R. C., and Lapina, K.: Large-scale impacts of anthropogenic pollution and boreal wildfires on the nitrogen oxides over the central North Atlantic region, J. Geophys. Res., 113, D17308, doi:10.1029/2007JD009689, 2008. 28387

Viezee, W. and Singh, H. B.: The distribution of beryllium-7 in the troposphere, implications on stratosphere/tropospheric air exchange, Geophys. Res. Lett., 7, 805–808, 1980. 28393

Vingarzan, R.: A review of surface ozone background levels and trends, Atmos. Environ., 38, 3431–3442, 2004. 28388

Wallace, J. and Gutzler, D. S.: Teleconnections in the geopotential height field during the Northern Hemisphere winter, Mon. Weather Rev., 109, 784–812, 1981. 28395

Wernli, H. and Bourqui, M.: A Lagrangian "1-year climatology" of (deep) cross-tropopause exchange in the extratropical Northern Hemisphere, J. Geophys. Res., 107, 4021, doi:10.1029/2001JD000812, 2002. 28405

WMO: Meteorology a Three-Dimensional Science: Second Session of the Commission for Aerology, WMO Bulletin IV(4), Tech. rep., NOAA Air Resources Laboratory, Geneva, 1957. 28392

Yienger, J. J., Klonecki, A. A., Levy II, H., Moxim, W. J., and Carmichael, G. R.: An evaluation of chemistry's role in the winter-spring ozone maximum found in the northern midlatitude free troposphere, J. Geophys. Res., 104, 3655–3667, doi:10.1029/1998JD100043, 1999. 28408

ACPD
12, 28385–28450, 2012

Table 1. Description of O_3 analyzers, associated quality assurance, and data acquisition system, used during the period 1988–2009. Ri = Reference instrument; Bi = Basic instrument; Bp = Backup instrument; MPC = Multipoint calibration.

Period	Instrument	Calibration system/ Quality Assurance	International Reference	Data acquisition
May 87–Jul 95	Dasibi-1008-AH #4283 (Bi)	Dasibi-1008-RS #5797 (Ri) MPC/ 2 months	NIST Traceable	Continuous Record: 10 min ± SD
Jul 95–Jul 96	Dasibi-1008-RS #5797 (Bi)		NIST Traceable	Continuous Record: 10 min ± SD
Jul 96–Feb 99	TEI 49C #55912-305(Bi) Dasibi-1008-RS #5797 (Bp)	EMPA Audit (Nov 96) TEI 49C-PS #56085-306 (Ri) (Apr 97) MPC/ 3 months EMPA Audit (Feb 98)	NIST-EMPA	Continuous Record: 1 min ± SD
Feb 99–Nov 03	TEI 49-C #62900-337(Bi) Dasibi-1008-RS #5797 (Bp)	TEI 49C-PS #56085-306(Ri) MPC/ 3 months EMPA Audit (Jun 00)	NIST-EMPA	Continuous Record: 1 min ± SD
Nov 03–Now	TEI 49-C #62900-337(Bi) TEI 49-C #72491-371(Bp)	TEI 49C-PS #56085-306(Ri) EMPA Audit (Nov 04) EMPA Audit (Nov 09)	NIST-EMPA	Continuous Record: 1 min ± SD

ACPD
12, 28385–28450, 2012

Table 2. Geographical sectors used in the backward trajectory classification (function of the continental source regions and oceanic sectors, latitude and longitude ranges).

Sector	Latitude Range	Longitude range
North America	30° N–90° N	50° W–135° W
North Atlantic	30° N–90° N	10.5° W–70° W
North Europe	50° N–90° N	10.5° W–50° E
South Europe	36° N–50° N	10.5° W–50° E
Sahara	20° N–36° N	18° W–50° E
Sahel	0° N–20° N	18° W–50° E
Subtropical North Atlantic	0° N–30° N	18° W–135° W
Canary Islands	24.7° N–31.9° N	12.4° W–20.6° W

ACPD
12, 28385–28450, 2012

Table 3. Basic statistics of surface O_3 at IZO for days with daily $^7Be > 8\,mBq\,m^{-3}$. The term "climat. O_3" refers to the O_3 mean when considering all the ozone values within the indicated period independently of the ^7Be value.

	Winter	Spring	Summer	Autumn
%cases/season	3.8	14.6	8.9	1.4
Mean O_3 (ppbv)	47.8 ± 1.9	60.3 ± 1.4	56.8 ± 2.2	46.3 ± 4.1
Median O_3 (ppbv)	45.0	59.4	56.8	42.3
Climat. O_3 (ppbv)	44.7 ± 0.3	53.6 ± 0.4	45.5 ± 0.5	40.4 ± 0.3

ACPD
12, 28385–28450, 2012

Table 4. O_3/CO ratios at IZO for events with hourly O_3-CO data correlation $r > 0.75$. Wi = winter; Sp = spring; Au = autumn.

	O_3 range (ppbv)	O_3/CO (ppbv/ppbv)	Cases(2008–2011)
Type 1	P75th–P100th: > 52	0.53 ± 0.09	100 % Sp
Type 2	P50th–P75th: 46–52	0.42 ± 0.06	54.5 % wi + 45.5 % Sp
Type 3	P25th–P50th: 40–46	0.46 ± 0.10	100 % Au
Type 4	P25th–P50th: < 40	0.35 ± 0.03	45.5 % Sp + 45.5 % Au

ACPD
12, 28385–28450, 2012

Table 5. Averaged O_3/CO ratios (ppbv ppbv^{-1}) at IZO for winter, spring, summer and autumn, and estimated type of air mass (FP = Fresh Pollution; A = Aged air mass; UT = Upper Troposphere). Types of air masses have been labelled according to the O_3/CO range values.

	Mean ± SD	Median	P25th	P75th	Air mass
Winter	0.39 ± 0.07	0.38	0.34	0.44	FP
O_3 > P75th	0.42 ± 0.06	0.40	0.37	0.45	FP
Spring	0.47 ± 0.10	0.46	0.40	0.53	A
O_3 > P75th	0.58 ± 0.10	0.56	0.51	0.62	A + UT
Summer	0.56 ± 0.15	0.55	0.44	0.65	A + UT
O_3 > P75th	0.71 ± 0.13	0.70	0.61	0.78	UT
Autumn	0.47 ± 0.10	0.47	0.41	0.54	A
O_3 > P75th	0.54 ± 0.08	0.54	0.49	0.60	A + UT

ACPD
12, 28385–28450, 2012

Table 6. Mean surface O_3 for NAO > +0.5 and NAO < −0.5 for each season in the period 1988–2009 with the corresponding standard deviation of the mean. The third column shows the confidence level for the difference between the means.

	A NAO > +0.5	B NAO < −0.5	Confidence Level
Winter	42.9 ± 0.3 (*n* = 605)	45.2 ± 0.3 (*n* = 349)	100.0 %
Spring	51.4 ± 0.5 (*n* = 440)	53.9 ± 0.6 (*n* = 362)	99.9 %
Summer	44 ± 0.7 (*n* = 366)	46.3 ± 0.6 (*n* = 456)	98.8 %
Autumn	40.3 ± 0.3 (*n* = 368)	40.8 ± 0.3 (*n* = 537)	76.2 %

ACPD
12, 28385–28450, 2012

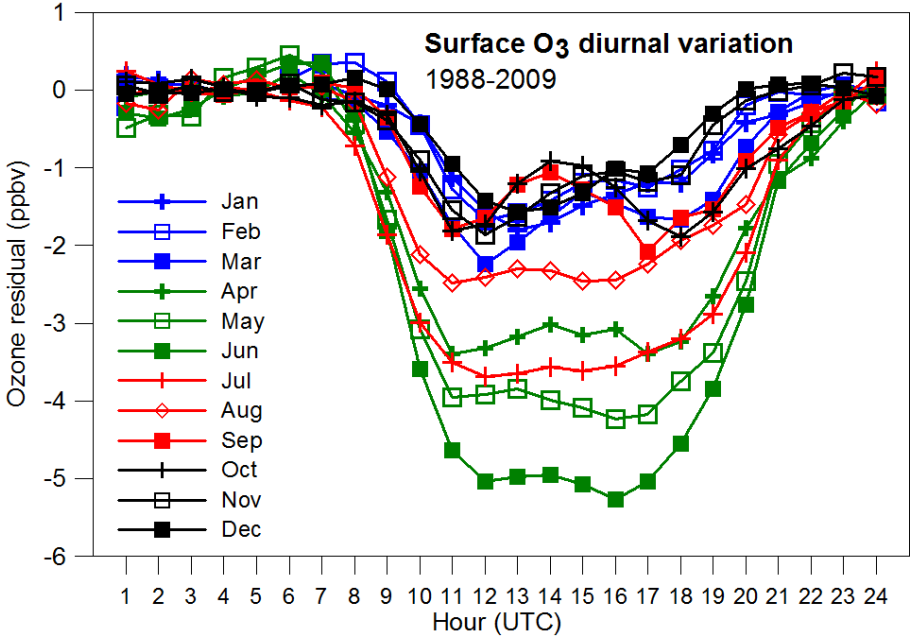

Fig. 1. Diurnal variation of surface O_3 residuals for each month of the year in the period 1988–2009. The O_3 residuals have been calculated on daily basis as the differences of surface O_3 for every hour over the night background level.

ACPD
12, 28385–28450, 2012

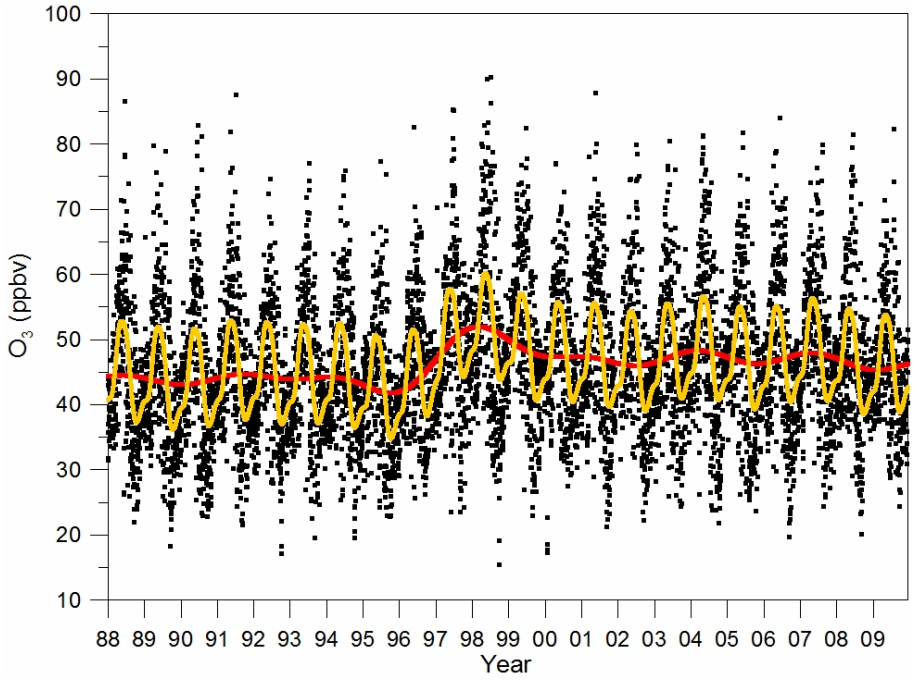

Fig. 2. Surface O_3 daily night means (black dots), inter-annual trend (red line) and inter-annual trend plus annual cycle at IZO from 1988 to 2009.

ACPD
12, 28385–28450, 2012

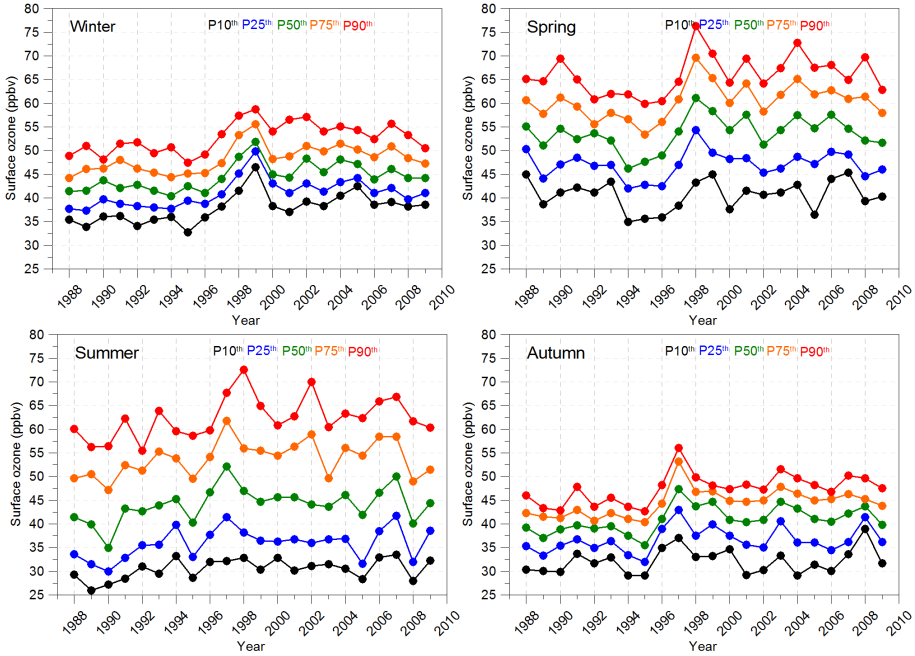

Fig. 3. Long-term (1988–2009) surface O_3 concentrations (night values: 22:00–06:00 UTC) for percentiles 10th, 25th, 50th, 75th, and 90th at IZO for winter (JFM), spring (AMJ), summer (JAS) and autumn (OND).

ACPD
12, 28385–28450, 2012

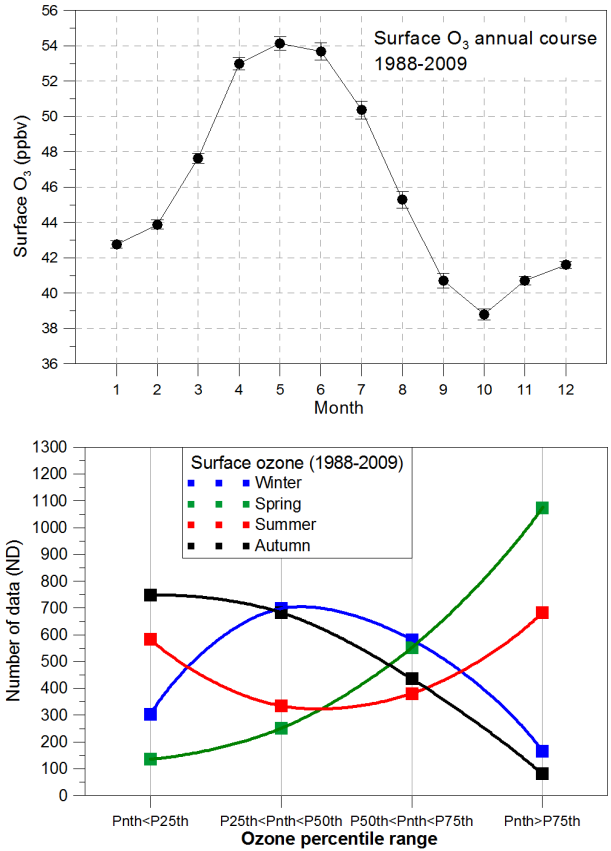

Fig. 4. Annual course of surface O_3 at IZO for the period 1988–2009 (top panel). Bars associated to monthly mean values are the standard deviation of the mean. In lower panel, the seasonal distribution of number of surface O_3 daily data (ND) within the following percentile ranges: P*n*th ≤ P10th, P10th < P*n*th ≤ P25th, P25th < P*n*th ≤ P50th, P50th < P*n*th ≤ P75th, P75th < P*n*th ≤ P90th and P*n*th > P90th.

ACPD
12, 28385–28450, 2012

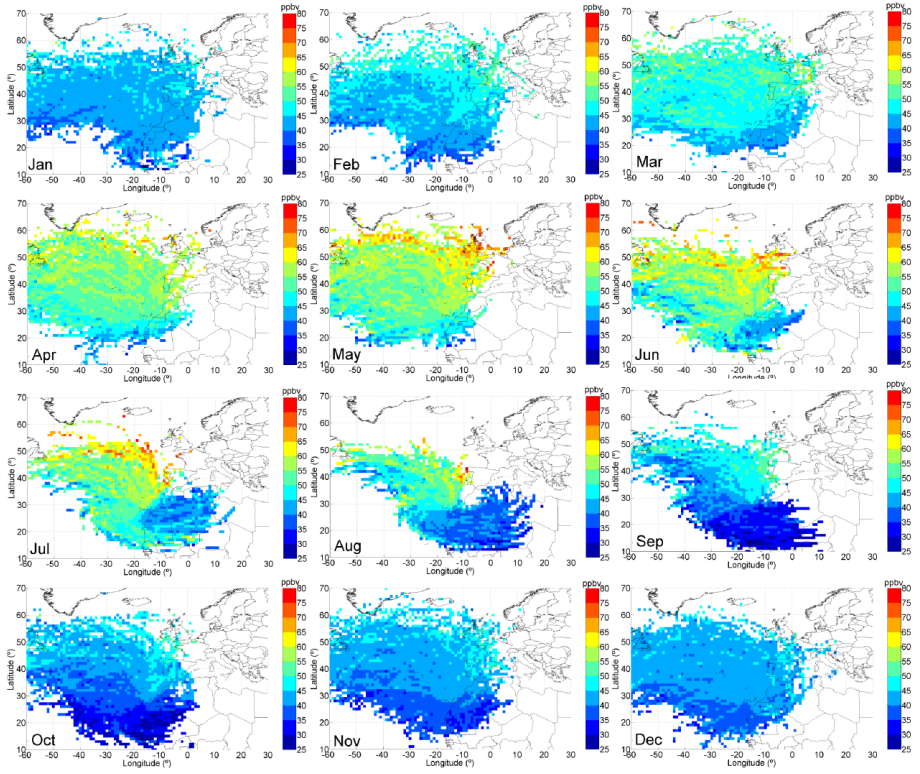

Fig. 5. Surface O_3 MCAR plots for each month of the year for the period 1988–2009. Color bars indicate O_3 concentration in ppbv.

ACPD
12, 28385–28450, 2012

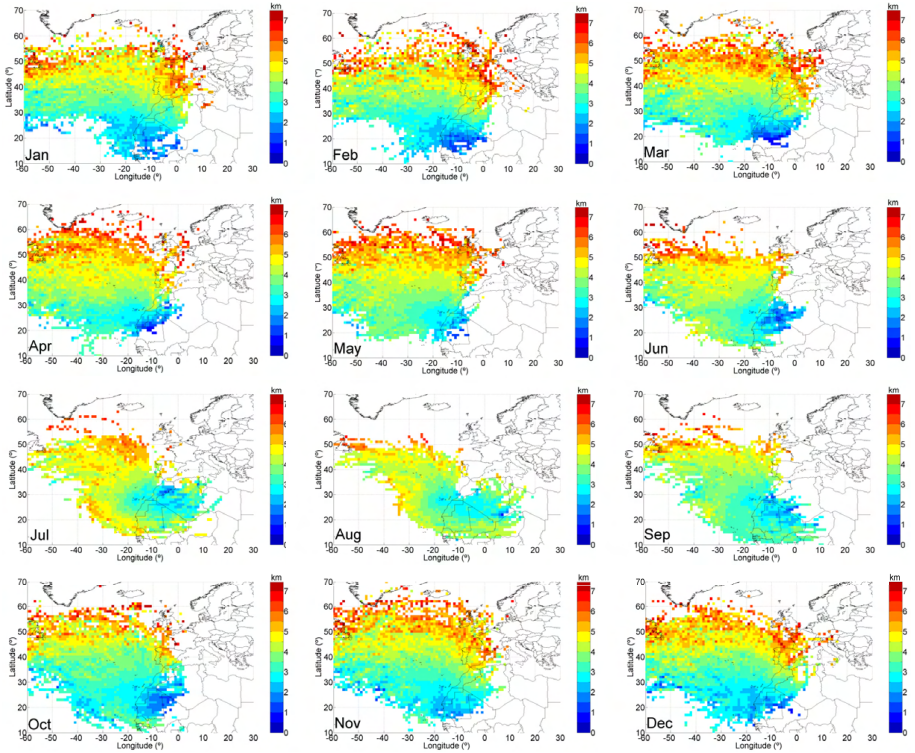

Fig. 6. Backward trajectory mean height plots for each month of the year for the period 1988–2009. Color bars indicate height in kilometers.

ACPD
12, 28385–28450, 2012

Surface O_3 characterization in the subtropical North Atlantic troposphere

E. Cuevas et al.

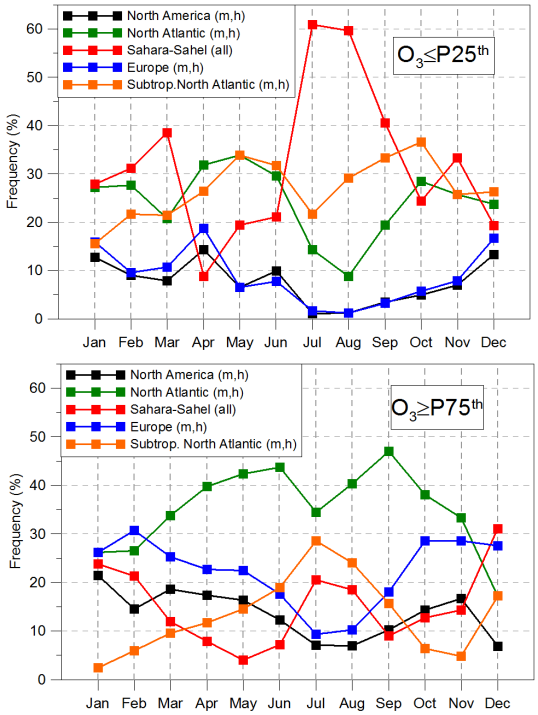

Fig. 7. Monthly mean percentage of air mass types arriving to IZO for O_3 < P25th for the period 1988–2009 (top panel); Monthly mean percentage of air mass types arriving to IZO for O_3 > P75th for the period 1988–2009 (bottom panel).

ACPD
12, 28385–28450, 2012

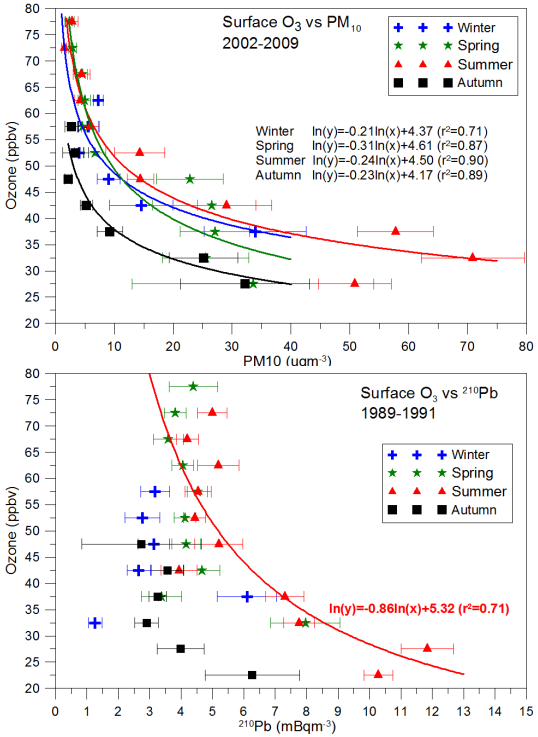

Fig. 8. PM_{10} (μm^{-3}) vs surface O_3 (ppbv) at IZO for winter (JFM), spring (AMJ), summer (JAS) and autumn (OND) in the period 2002–2009 (top panel); ^{210}Pb ($mBq\,m^{-3}$) vs. surface O_3 (ppbv) for the same seasons in the period 1988–1991 (bottom panel). SurfaceO_3 daily nocturnal data have been grouped in 10 ppbv bin ranges from the minimum to maximum value. Each point of the plot represents the median value of surface O_3 concentrations associated to the mean values of PM_{10} or ^{210}Pb in a determined bin range. The standard deviation of the mean (SDOM) associated to PM_{10} and ^{210}Pb mean values is represented by horizontal bars.

ACPD
12, 28385–28450, 2012

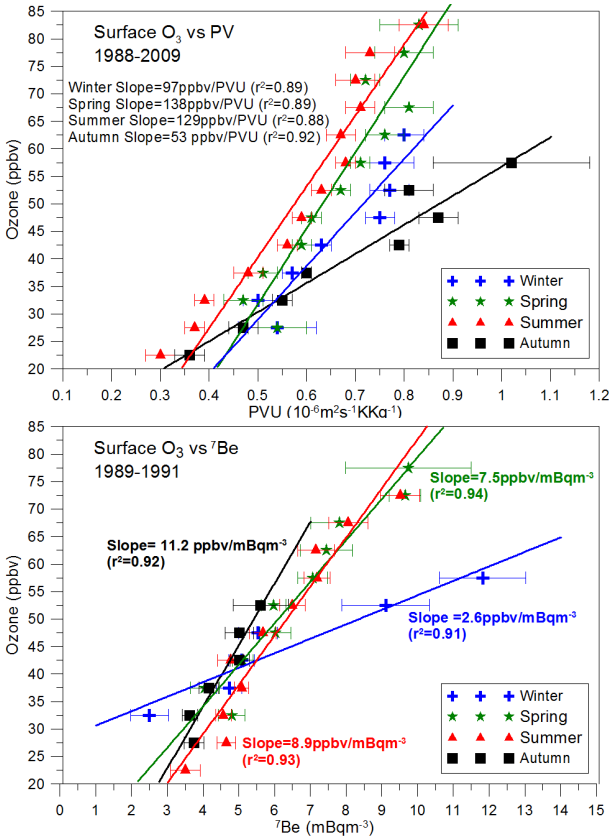

Fig. 9. PV_{max} (1 PVU = 10^{-6} m^2 s^{-1} K Kg^{-1}) vs. surface O_3 (ppbv) at IZO for winter (JFM), spring (AMJ), summer (JAS) and autumn (OND) in the period 1988–2009 (top panel); ^{7}Be (mBq m^{-3}) vs. O_3 ozone (ppbv) at IZO for the same seasons in the period 1989–1991 (bottom panel). Data have been grouped and depicted as for Fig. 8.

ACPD
12, 28385–28450, 2012

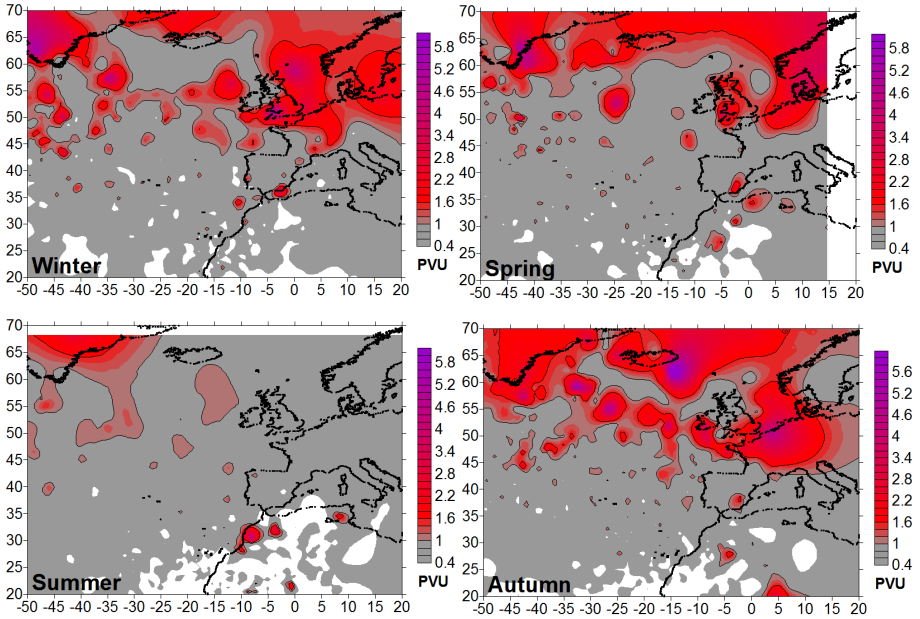

Fig. 10. PV_{max} maps for winter (JFM), spring (AMJ), summer (JAS) and autumn (OND) in the period 1988–2009. They have been constructed from the coordinates of PV_{max} values found by 5-day backward trajectories arriving at IZO every day at 00:00 UTC in ECMWF PV-reanalysis fields. Thresholds of 1 and 1.6 PVU are marked with black lines.

ACPD
12, 28385–28450, 2012

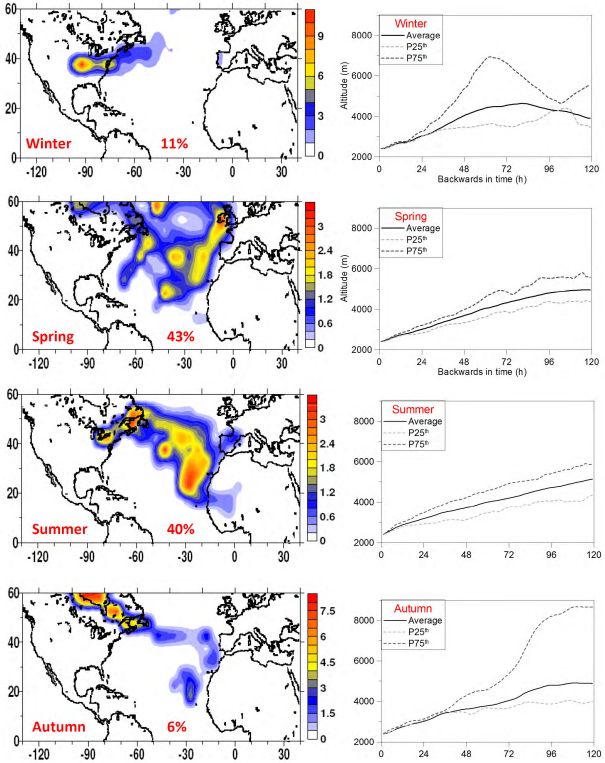

Fig. 11. Residence times and transport pathways of air masses with daily $^{7}Be > 8\,mBq\,m^{-3}$ and corresponding averaged backward trajectories heights for each season of the year. Color bars indicate the residence time in arbitrary units. In backward trajectory heights the mean value, P25th and P75th are plotted.

ACPD
12, 28385–28450, 2012

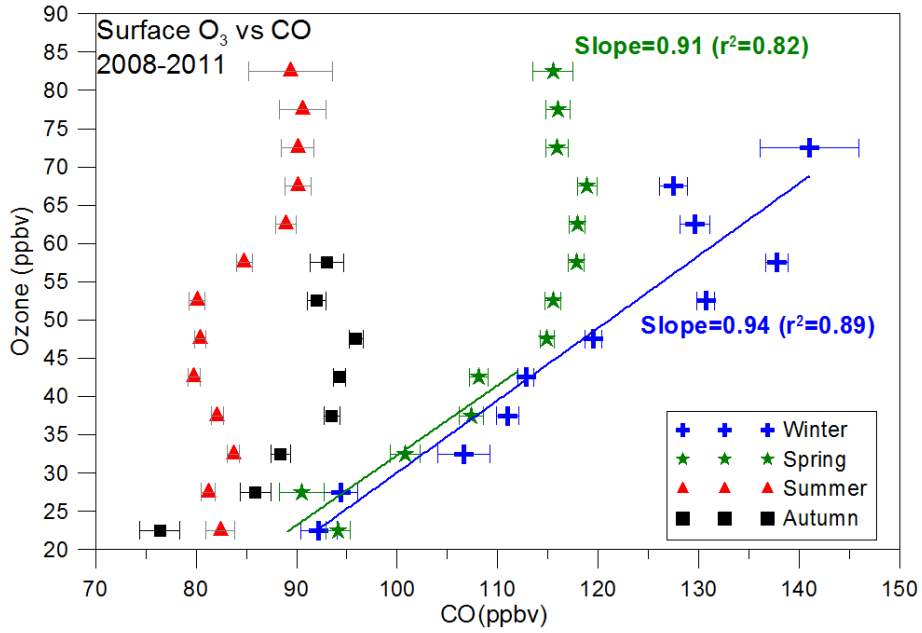

Fig. 12. CO (ppbv) vs. surface O_3 (ppbv) at IZO for winter (JFM), spring (AMJ), summer (JAS) and autumn (OND) in the period 2008–2011. Data have been grouped and depicted as for Fig. 8.

ACPD
12, 28385–28450, 2012

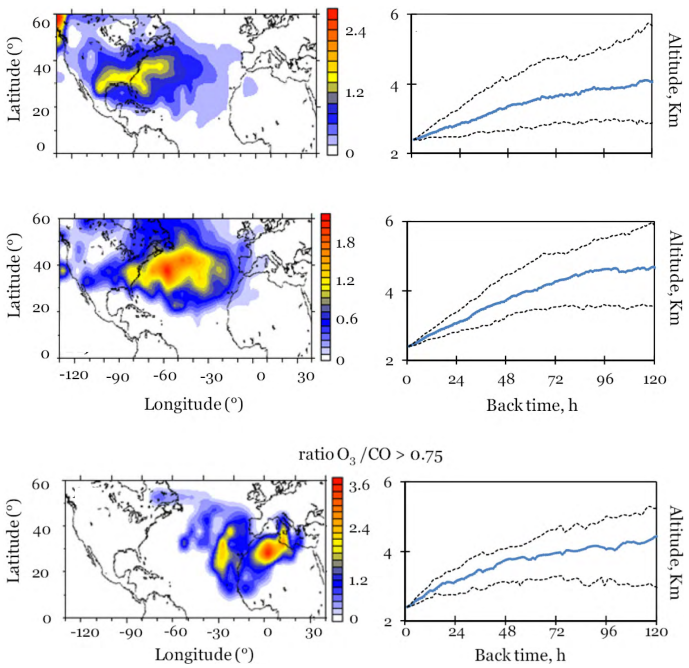

Fig. 13. Residence time of air masses (corrected by central convergence) that show an O_3-CO hourly correlation $r > 0.75$ for winter and spring (top and middle panels, in the left). Color bars indicate residence time in arbitrary units. In the right, mean, P25th and P75th of 5-day backward air masses travelling altitude for these events in winter and spring are depicted; residence time of air masses that show an O_3/CO hourly ratio > 0.75 ppbv ppbv^{-1} (bottom panels).

ACPD
12, 28385–28450, 2012

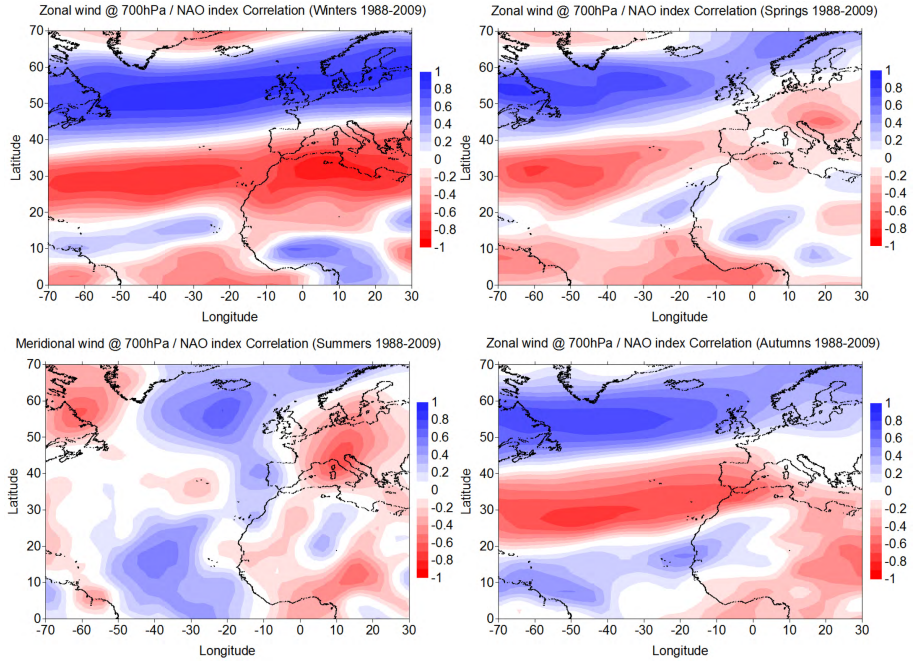

Fig. 14. Correlation between zonal wind component (u) at 700 hPa and NAO-index in winter (JFM), spring (AMJ), summer (JAS) and autumn (OND) for the period 1988–2009.

ACPD
12, 28385–28450, 2012

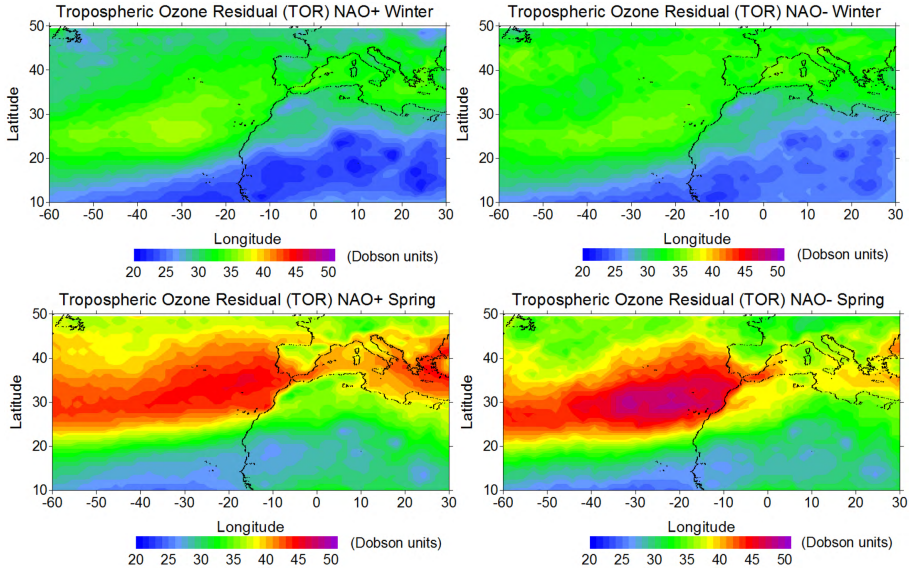

Fig. 15. Averaged Tropospheric Ozone Residual (TOR) data (in Dobson units) in winter (JFM) and spring (AMJ) for years with NAO > +0.5 and for years with NAO < −0.5, respectively.

ACPD
12, 28385–28450, 2012

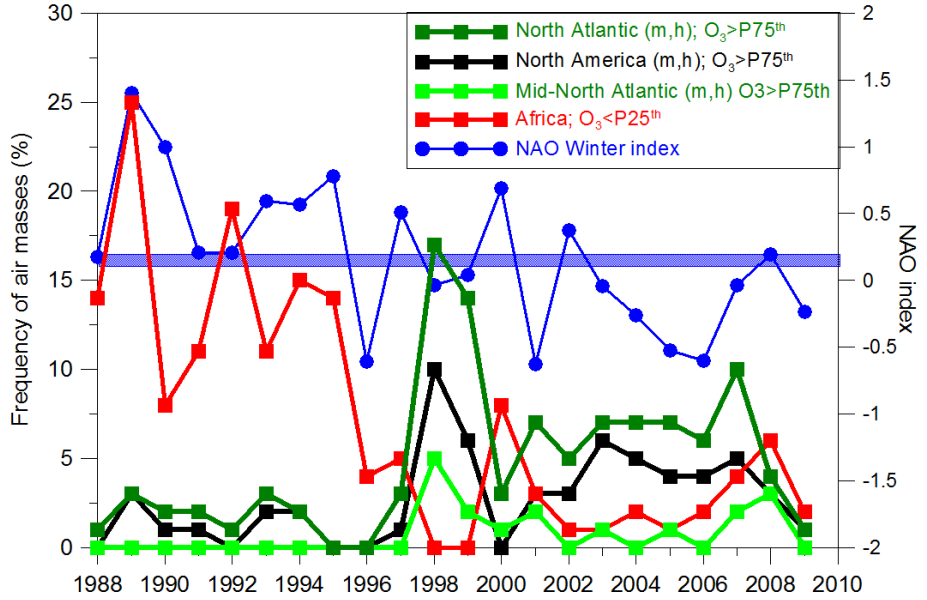

Fig. 16. Long term frequency of air masses arriving to IZO from Africa sector associated with O_3 < P25th, and from North Atlantic and North America associated with O_3 > P75th in winter. NAO index for winter is also shown.

ACPD
12, 28385–28450, 2012